Supramolecular Cuboctahedra with Aggregation-Induced Emission Enhancement and External Binding Ability

Zhe Zhang[a⊥], Qixia Bai[a⊥], Erendra Manandhar[c⊥], Yunting Zeng[b], Tun Wu[a], Ming Wang[b], Liao-Yuan Yao[d], George R. Newkome[c*], Pingshan Wang[a*], Ting-Zheng Xie[a*]

[a] Institute of Environmental Research at Greater Bay Area; Key Laboratory for Water Quality and Conservation of the Pearl River Delta, Ministry of Education; Guangzhou Key Laboratory for Clean Energy and Materials, Guangzhou University, Guangzhou-510006, China

[b] State Key Laboratory of Supramolecular Structure and Materials, College of Chemistry, Jilin University, Changchun, Jilin 130012, China

[c] Departments of Polymer Science and Chemistry, University of Akron, Akron, OH 44325-4717, USA

[d] MOE Key Laboratory of Cluster Science, School of Chemistry and Chemical Engineering, Beijing Institute of Technology, Beijing 102488, China

Table of content

1. Schemes of preparation of ligands

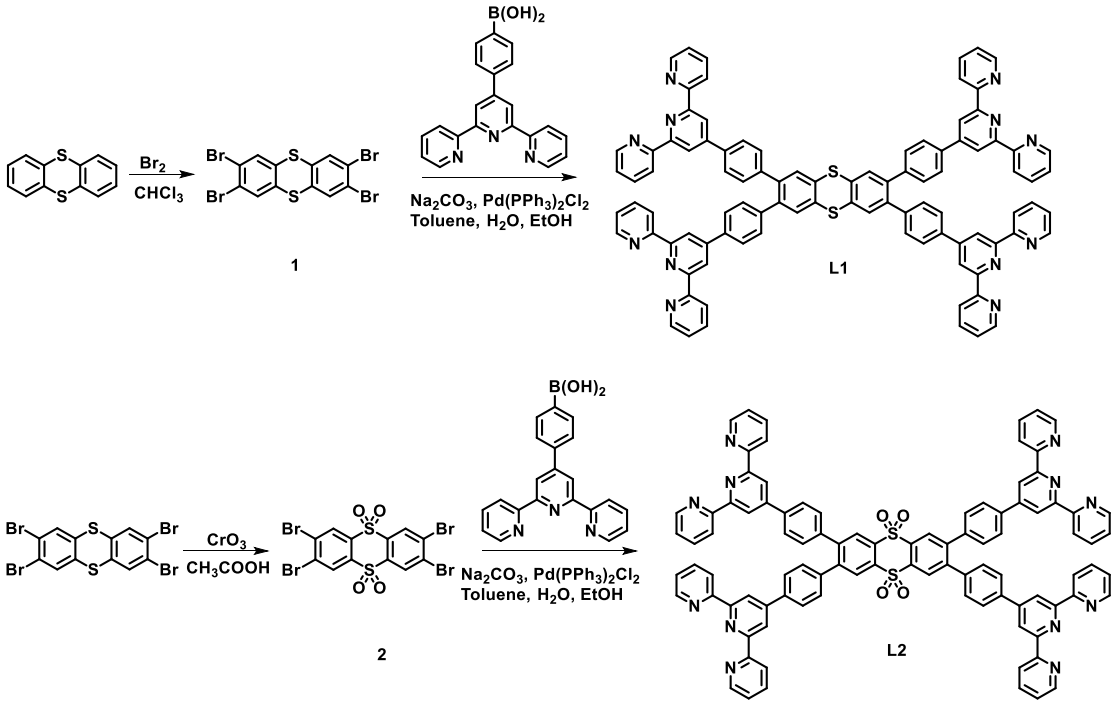

Scheme S1. Synthesis route of ligand **L1 and L2**

2. Experimental section

General Procedures. Reagents and solvents were purchased from Energy Chemical, Bidepharm and used without purification. Thin layer chromatography (TLC) was performed on flexible sheets (Greagent) precoated with Al_2O_3 (IB-F) and SiO_2 (IB2-F) and visualized by UV light. Column chromatography was conducted using neutral Al_2O_3 (200-300 mesh) SiO_2 (200-300 mesh). ^1H, ^{13}C, 2D COSY, 2D ^1H-^1H NOESY NMR and 2D DOSY NMR spectra were recorded on a Bruker NMR 400, 500, 600 MHz. Different NMR solvents were purchased from J&K scientific and Sigma/Aldrich. ESI-MS and TWIM-MS were recorded with a Waters Synapt G2-Si tandem mass spectrometer, using solutions of 0.01 mg sample in 1 mL of $CHCl_3$/CH_3OH (1:3, *v/v*) for ligands or 0.5 mg sample in 1 mL of DMF/MeOH (3:1, *v/v*) for complexes.

TWIM-MS. The TWIM-MS experiments were performed under the following conditions: ESI capillary voltage, 2 kV; sample cone voltage, 35 V; source offset, 42V; source temperature 150 °C; desolvation temperature, 250 °C; cone gas flow, 10 L/ h; desolvation gas flow, 700 L/h (N_2); source gas flow, 0 mL/min; trap gas flow, 3 mL/min;

helium cell gas flow, 120 mL/min; ion mobility (IM) cell gas flow, 30 mL/min; sample flow rate, 8 μL/min; IM traveling wave height, 25 V; and IM traveling wave velocity, 1200 m/s. Q was set in rf-only mode to transmit all ions produced by ESI into the triwave region for the acquisition of TWIM-MS data. Data were collected and analyzed by using Mass Lynx 4.2 and Drift Scope 2.9.

gMS^2. Gradient tandem mass spectrometry was performed under the following conditions:17+ charged ions of complexes, 17+ charged ions of **S1 (S2) ⊃ G** were isolated by quadrupole for the following collision induced dissociation (CID), in which collision energy was gradually increased by changing the voltage of trap cell depended on different complexes.

TEM. Transmission electron microscopy tests were performed on the JEOL JEM-2100F equipment. The sample solutions were drop-casted on to a lacey carbon covered Cu grid (300 mesh, purchased from Beijing Zhongjingkeyi Technology Co., Ltd.) and the extra solution was absorbed by filter paper to avoid aggregation.

AFM. AFM imaging was performed on a Bruker Dimension Icon AFM system with ScanAsyst and the data was processed by NanoScope Analysis version 2.0 (Bruker Software, Inc.) The sample was diluted to a concentration of 10^{-6} M using DMF, dropped on freshly cleaved mica surface, and then dried in the air. Silicon cantilevers tip with spring constant of around 0.1 N/m was used for the experiments.

DLS. Dynamic light scattering (DLS) was carried out on a Nano-ZS90 instrument at room temperature. The sample was diluted to a concentration of 10^{-6} M using DMF.

Molecular Modeling. Energy minimization of the macrocycles was conducted with the Materials Studio version 6.0 program, using the Anneal and Geometry Optimization tasks in the Forcite module (Accelrys Software, Inc.). The counterions were omitted.

UV-vis absorption and fluorescence properties. UV-vis absorption spectra were recorded on a Thermo Fisher Scientific Evolution 201 spectrophotometer at room temperature (0.5 μM in $CHCl_3$ or DMF) and were corrected with the background spectrum of the solvent. Fluorescence properties were performed on HITACHI Exciter F-4600 at room temperature. (1 μM in $CHCl_3$ or DMF).

Single crystal X-ray diffraction. Structural confirmation of **L1** and **L2** were provided by X-ray crystallographic analysis. Single crystal X-ray diffraction data for **L1** and **L2** were collected on a XtaLAB Synergy diffractometer using a mirror monochromated Cu-Kα radiation. Two suitable crystals of **L1 and L2** were selected and texted on Bruker P4 diffractometer. These crystals were kept at 100.00 K corresponding to **L1 and L2** during data collection. Using Olex2, the structures were solved with the SIR2004 [2] structure solution program using Direct Methods and refined with the XH [3] refinement package using CGLS minimisation. The structures were solved by direct methods and refined by full-matrix least-squares on F^2 with anisotropic displacement using the SHELXTL software package. Details on crystal data collection and refinement were summarized in Table S3. CCDC: 2132604 (**L1**), 2132525 (**L2**).

3. Synthesis of the compounds and supramolecules

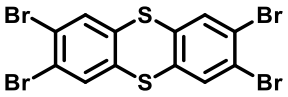

Compound 1: To a stirred solution of thianthrene (2.2 g, 10.0 mmol) in CH_2Cl_2 (60 mL) at 0 °C, a solution of Br_2 (19.2 g, 120 mmol) in CH_2Cl_2 (10 mL) was added drop-wise. After stirring at 25 °C for 48 h, the reaction mixture was washed with saturated Na_2SO_3 solution until colorless, dried over anhydrous $MgSO_4$, and then concentrated in vacuo to give the product as 3.20 g white solid (yield: 60%). ^{1}H NMR (500 MHz, $CDCl_3$, 300 K): δ = 7.23 (s, 4 H, Ph-H^a). ^{13}C NMR (100 MHz, $CDCl_3$, 300 K): δ = 138.91, 132.44, 125.27.[1-2] ESI-TOF (*m/z*): Calcd. for [$C_{12}H_4Br_4S_2$+H^+]=532.90, Found: 532.91.

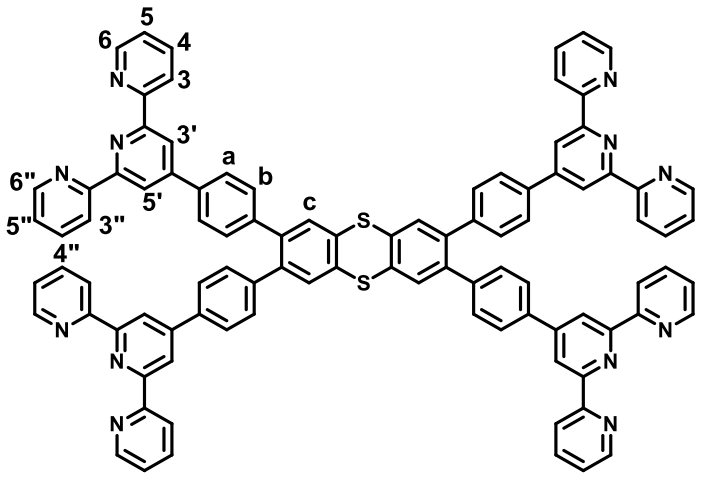

L1: The mixture of compound **1** (595.9 mg, 1 mmol), 4′-(4-boronatophenyl)-2,2′:6′,2″-terpyridine (2.12 g, 6 mmol), Na_2CO_3 (1.27 g, 12 mmol), and $Pd(PPh_3)_2Cl_2$ (140.2 mg, 0.2 mmol) in the solution of MeOH (80 mL), H_2O (120 ml) and toluene (200 mL) were refluxed for 96 h under N_2. After separating the toluene layer, the aqueous layer was extracted with CH_2Cl_2 (3×50 mL). The combined organic layers were dried with $MgSO_4$, and concentrated in vacuo. The residue was washed with methanol, collected and crystallized in $CHCl_3$ and methanol to give pure light blue solid: 896.0 mg (yield: 65%); ^{1}H NMR (500 MHz, $CDCl_3$, 298 K, ppm) 8.81 (s, 8H, tpy-$H^{3',5'}$), 8.67 (d, $J_{6,6''\text{-}5,5''}$= 4.8 Hz, 8H, tpy-$H^{6,6''}$), 8.6 (d, $J_{3,3''\text{-}4,4''}$= 8.5 Hz, 8H, tpy-$H^{3,3''}$), 7.85 (d, $J_{a\text{-}b}$ = 8.4 Hz, 8H, Ph-H^a), 7.80 (m, 8H, tpy-$H^{4,4''}$), 7.73 (s, 4H, Ph-H^c), 7.37 (d, $J_{b\text{-}a}$ = 8.7 Hz, 8H, Ph-H^b), 7.34 (m, 8H, tpy-$H^{5,5''}$). ^{13}C NMR (100 MHz, $CDCl_3$, ppm): δ 156.10, 156.05,

149.09, 149.03, 138.77, 138.55, 138.39, 136.77, 136.07, 129.00, 128.26, 128.22, 125.24, 123.78, 121.28, 118.84. ESI-TOF (*m/z*): Calcd. for [$C_{96}H_{60}N_{12}S_2$] = 1445.77, Found: 1445.78.

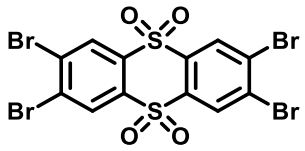

Compound 2: A solution of compound **1** and excess chromic oxide in acetic acid was heated at 100℃ for 24 h. It was then cooled and the resulting white solid was collected by filtration. The compound is difficult to purify by the column as it is insoluble in most of the solvents and used without further purification for next step.[3-4] ESI-TOF (*m/z*): Calcd. for [$C_{12}H_4Br_4O_4S_2$+Na^+]=618.89, Found: 618.92.

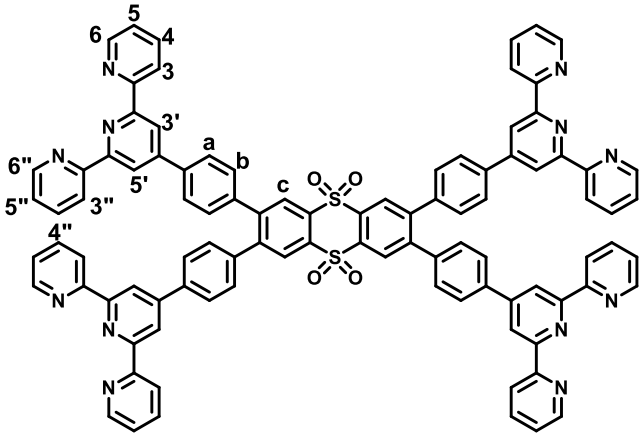

L2: The mixture of compound **2** (537.5 mg, 1 mmol), 4′-(4-boronatophenyl)-2,2′:6′,2″-terpyridine (1.91 g, 6 mmol), Na_2CO_3 (1.145 g, 12 mmol), and $Pd(PPh_3)_2Cl_2$ (208.1 mg, 0.2 mmol) in the solution of EtOH (80 mL), H_2O (120 mL) and toluene (200 mL) was refluxed for 48 h under Ar. After separating the toluene layer, the aqueous layer was extracted with $CHCl_3$ (150 mL, 3×50 mL). The combined organic layers were dried ($MgSO_4$), and concentrated in vacuo. The residue was washed with methanol, collected and crystallized in methanol to give pure light blue solid: 896.0 mg; ^{1}H NMR (500 MHz, $CDCl_3$, 298 K, ppm) 8.74 (s, 8H, tpy-$H^{3',5'}$), 8.68 (d, $J_{6,6''\text{-}5,5''}$= 4.8 Hz, 8H, tpy-$H^{6,6''}$), 8.64 (d, $J_{3,3''\text{-}4,4''}$= 8.5 Hz, 8H, tpy-$H^{3,3''}$), 8.44 (s, 4H, Ph-H^c), 7.90 (d, $J_{a\text{-}b}$ = 8.4 Hz, 8H, Ph-H^a), 7.84 (m, 8H, tpy-$H^{4,4''}$), 7.38 (d, $J_{b\text{-}a}$ = 8.7 Hz, 8H, Ph-H^b), 7.32 (m, 8H, tpy-$H^{5,5''}$). ^{13}C NMR (125 MHz, $CDCl_3$, ppm): δ 156.10, 156.05, 149.09, 149.03, 138.77, 138.55, 138.39, 136.77, 136.07, 129.00, 128.26, 128.22, 125.24, 123.78, 121.28, 118.84**.**

ESI-TOF (*m/z*): Calcd. for [$C_{96}H_{60}N_{12}O_4S_2$] =1509.71, Found: 1509.73.

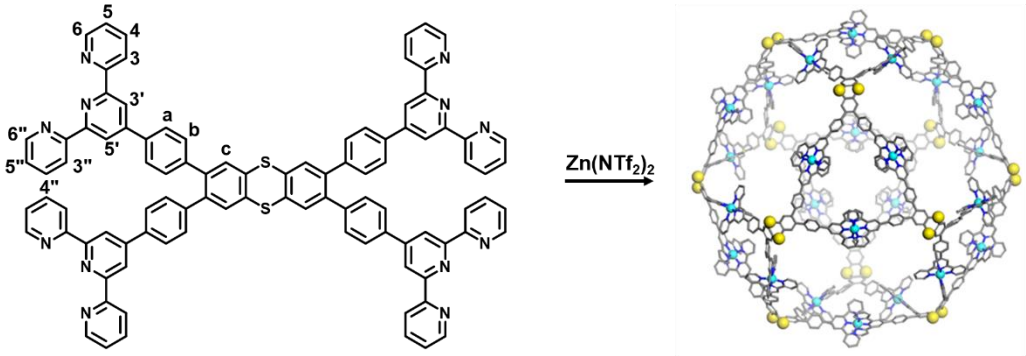

S1: A methanol solution of $Zn(NTf_2)_2$ (37.63 mg, 0.06 mmol) was added slowly drop by drop into a stirred solution of **L1** (42.0 mg, 0.03 mmol) in $CHCl_3$ and MeOH (1:1, 20 mL). The mixture was stirred at 55ºC for 8 h, then 10-fold excess $LiNTf_2$ was added for the anion exchange. The residue was filtered, washed with water (10 mL × 3) and MeOH (10 mL × 3), and dried *in vacuo* to give complex **3**, as pale yellow solid (76.8 mg，98%), ESI-TOF (*m/z*): 2662.14 $[M-11\ NTf_2^-]^{11+}$ (calcd *m/z*: 2662.14), 2416.89 $[M-12NTf_2^-]^{12+}$ (calcd *m/z*: 2416.89), 2209.45 $[M-13NTf_2^-]^{13+}$ (calcd *m/z*: 2209.45), 2031.63 $[M-14NTf_2^-]^{14+}$ (calcd *m/z*: 2031.63), 1877.53 $[M-15NTf_2^-]^{15+}$ (calcd *m/z*: 1877.53), 1742.69 $[M-16NTf_2^-]^{16+}$ (calcd *m/z*: 1742.69), 1623.65 $[M-17NTf_2^-]^{17+}$ (calcd *m/z*: 1623.65), 1517.90 $[M-18NTf_2^-]^{18+}$ (calcd *m/z*: 1517.90), 1423.28 $[M-19NTf_2^-]^{19+}$ (calcd *m/z*: 1423.28), 1338.12 $[M-20NTf_2^-]^{20+}$ (calcd *m/z*: 1338.12); ^{1}H NMR (500 MHz, CD_3CN/DMF-d_7 (v/v, 4:1), 298 K, ppm) 9.01 (s, 96H, tpy-$H^{3',5'}$), 8.73 (d, $J_{3,3''\text{-}4,4''}$= 8.5 Hz, 96H, tpy- $H^{3,3''}$), 8.18 (d, $J_{a\text{-}b}$ = 8.1 Hz, 96H, Ph-H^a), 8.09 (m, 96H, tpy-$H^{4,4''}$), 8.01 (s, 48H, Ph-H^c), 7.85 (d, $J_{6,6''\text{-}5,5''}$= 4.5 Hz, 96H, tpy-$H^{6,6''}$), 7.66 (d, $J_{b\text{-}a}$ = 8.6 Hz, 96H, Ph-H^b), 7.36 (m, 96H, tpy-$H^{5,5''}$).

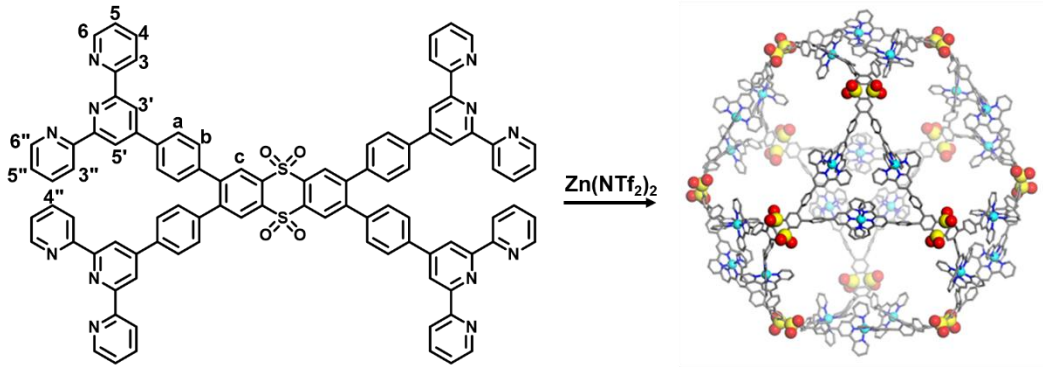

S2: A methanol solution of $Zn(NTf_2)_2$ (22.88 mg, 0.04 mmol) was added slowly drop by drop into a stirred solution of **L2** (27.2 mg, 0.02 mmol) in $CHCl_3$ and MeOH (1:1,

20 mL). The mixture was stirred at 55ºC for 8 h, then 10-fold excess $LiNTf_2$ was added for the anion exchange. The residue was filtered, washed with water (10 mL × 3) and MeOH (10 mL× 3), and dried *in vacuo* to give complex **3**, as light blue solid (48.7 mg，98%), ESI-TOF (*m/z*): 2731.95 $[M-11NTf_2^-]^{11+}$ (calcd *m/z*: 2731.95), 2840.95 $[M-12NTf_2^-]^{12+}$ (calcd *m/z*: 2840.95), 2268.50 $[M-13NTf_2^-]^{13+}$ (calcd *m/z*: 2268.50), 2086.48 $[M-14NTf_2^-]^{14+}$ (calcd *m/z*: 2086.48), 1928.71 $[M-15NTf_2^-]^{15+}$ (calcd *m/z*: 1928.71), 1790.68 $[M-16NTf_2^-]^{16+}$ (calcd *m/z*: 1790.68), 1668.82 $[M-17NTf_2^-]^{17+}$ (calcd *m/z*: 1668.82), 1560.56 $[M-18NTf_2^-]^{18+}$ (calcd *m/z*: 1560.56), 1643.68 $[M-19NTf_2^-]^{19+}$ (calcd *m/z*: 1643.68), 1376.51 $[M-20NTf_2^-]^{20+}$ (calcd *m/z*: 1376.51); ^1H NMR (500 MHz, CD_3CN/DMF-d_7 (*v/v*, 4:1), 298 K, ppm) 9.02 (s, 96H, tpy-$H^{3',5'}$), 8.75 (d, $J_{3,3''-4,4''}$= 8.9 Hz, 96H, tpy- $H^{3,3''}$), 8.62 (s, 48H, Ph-H^c), 8.24 (d, J_{a-b} = 7.3 Hz, 96H, Ph-H^a), 8.10 (m, 96H, tpy-$H^{4,4''}$), 7.86 (d, $J_{6,6''-5,5''}$= 4.5 Hz, 96H, tpy-$H^{6,6''}$), 7.74 (d, J_{b-a} = 7.5 Hz, 96H, Ph-H^b), 7.38 (m, 96H, tpy-$H^{5,5''}$).

4. Synthesis of Porphyrin Zn

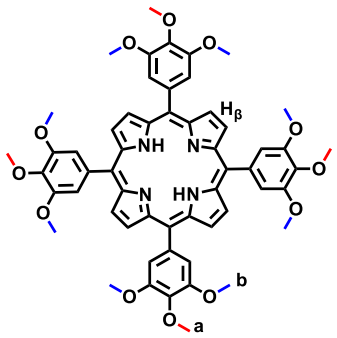

5,10,15,20-tetrakis(3,4,5-trimethoxyphenyl) porphyrin.[5-7] In a three-necked round bottom flask, a mixture of the 3,4,5-trimethoxybenzaldehyde (2.00 g, 10.19 mmol), and pyrrole (0.67 g, 10.19 mmol), $BF_3 \cdot Et_2O$ (498 µL, 4.08 mmol) were added to 500 mL dichloromethane and 5 mL ethanol. The mixture was stirred at room temperature for 120 mins then 2,3-dicloro-5,6-diciano-1,4-benzoquinona (DDQ) (2.28 g, 10.19 mmol) was added and kept the solution stirring for 4 h. In the end, triethylamine (5.7 mL, 40.76 mmol) was injected into the obtained solution. The mixture was concentrated to 80 mL under reduced pressure. The crude product was purified was subjected to column chromatography on SiO_2 with dichloromethane and concentrated under reduced pressure. Expected compound was obtained as a purple solid (373 mg, yield 15%) after washing with acetone and dried. ^{1}H NMR (400 MHz, 298 K, $CDCl_3$) δ 8.96 (s, 8H, H^{β}-pyrro), 7.47 (s, 8H, *Ph*), 4.18 (s, 12H, $-OCH_3^{a}$), 3.97 (s, 24H, $-OCH_3^{b}$), -2.78 (s, 2H, –NH). ^{13}C NMR (100 MHz, DMSO-d_6) δ 151.67, 138.04, 137.24, 120.33, 113.31, 60.92, 56.72, 31.12. ESI-TOF (*m/z*): Calcd. for [$C_{56}H_{54}N_4O_{12} + H^+$]: 976.06. Found:976.10.

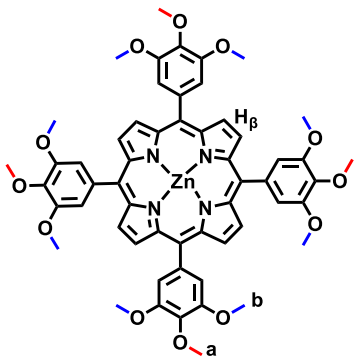

5,10,15,20-tetrakis(3,4,5-trimethoxyphenyl) porphyrin zinc (Guest). In a round bottom flask, 5,10,15,20-tetrakis(3,4,5-trimethoxyphenyl) porphyrin (100 mg, 0.10 mmol) was dissolved in 60 mL chloroform and a solution of $Zn(OAc)_2$ (55 mg, 0.30

mmol) in 8 mL methanol was added. The reaction mixture was stirred at room temperature for 8 h. The crude product was concentrated under reduced pressure and the residue was washed with methanol and dried under vacuum to get the dark purple solid (97.9 mg, 92%). ^{1}H NMR (400 MHz, 298 K, DMSO-d_6) δ 8.94 (s, 8H, H$^{\beta}$-pyrro), 7.51 (s, 8H, *Ph*), 4.00 (s, 12H, –OCH_3^a), 3.90 (s, 24H, –OCH_3^b). ^{13}C NMR (100 MHz, DMSO-d_6) δ 151.35, 149.79, 138.77, 137.71, 132.10, 120.59, 113.25, 60.93, 56.67. ESI-TOF (*m/z*): Calcd. for [$C_{56}H_{52}N_4O_{12}Zn$]: 1038.43. Found:1038.46.

5. ^{1}H NMR, ^{13}C NMR, 2D COSY NMR, 2D NOESY NMR, 2D DOSY NMR

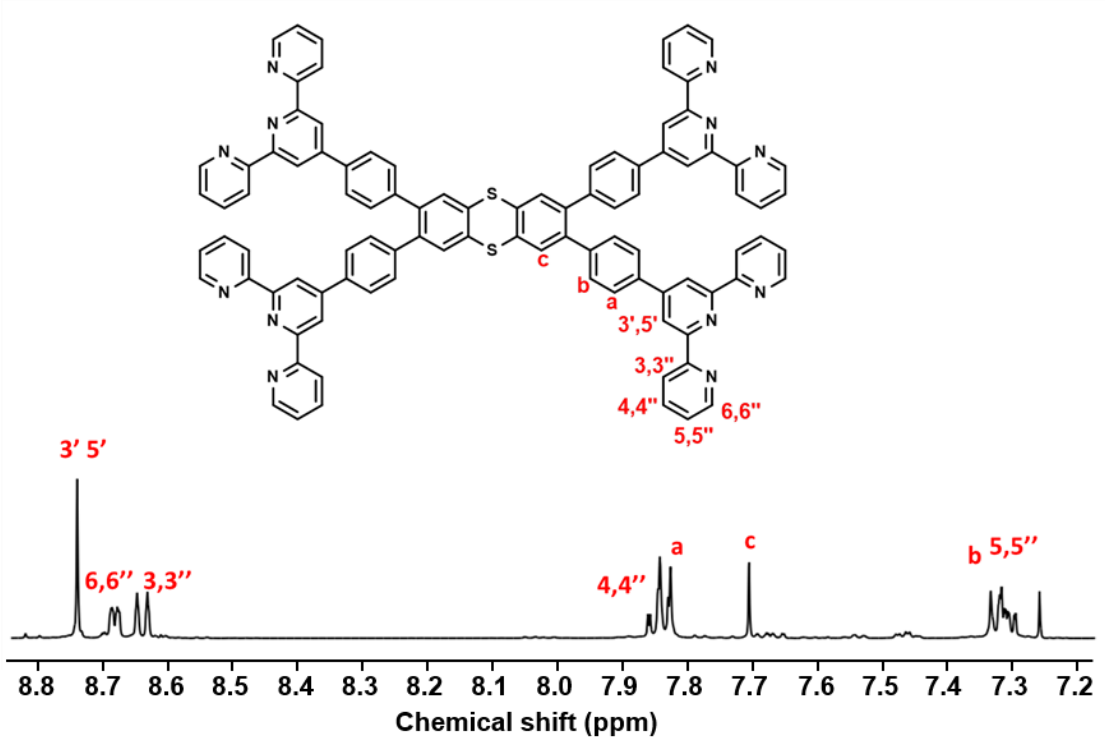

Figure S1. ^{1}H NMR spectrum (500 MHz, 298 K) of **L1** in $CDCl_3$.

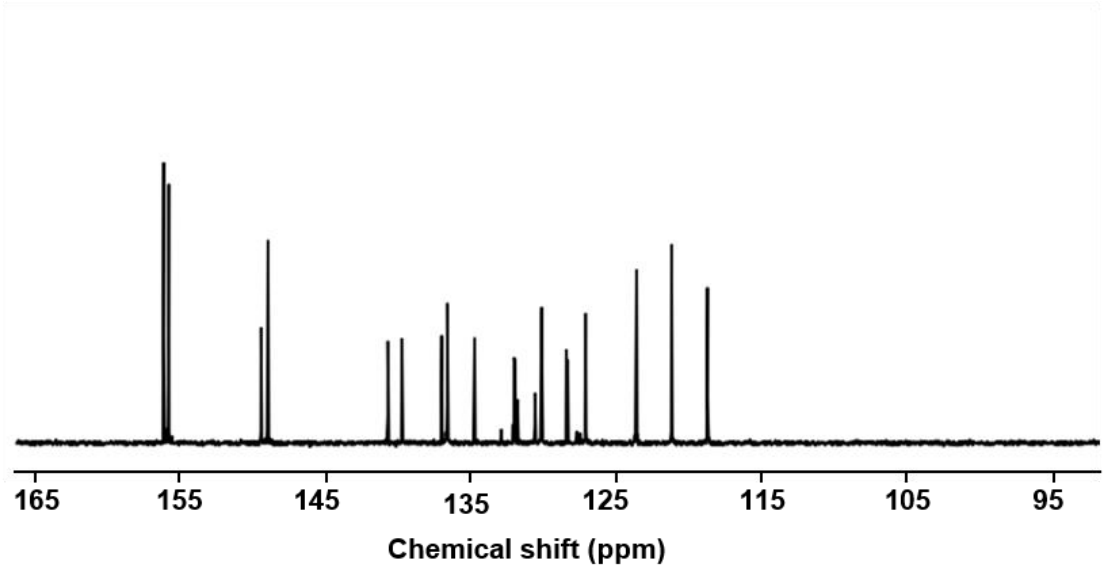

Figure S2. ^{13}C NMR spectrum (125 Hz, 298 K) of **L1** in $CDCl_3$.

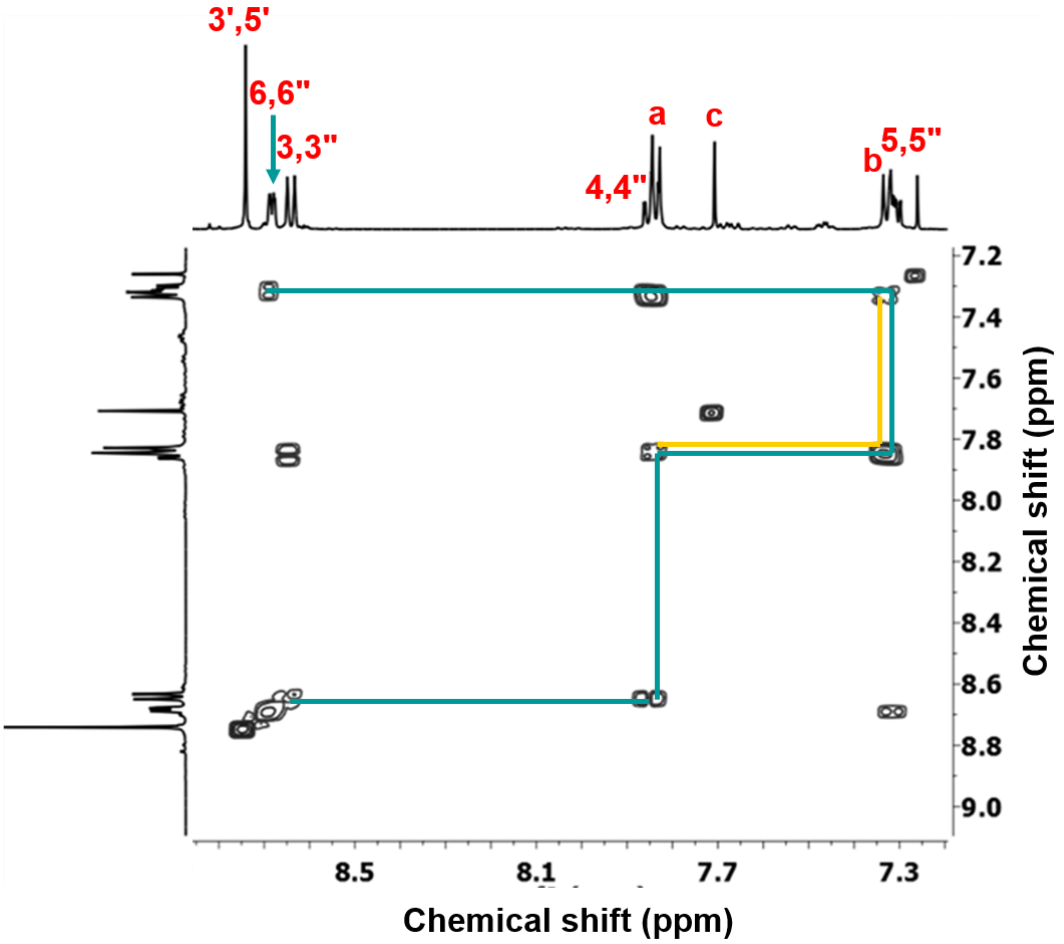

Figure S3. 2D ^{1}H-^{1}H COSY spectrum (500 MHz, 298 K) of **L1** in $CDCl_3$.

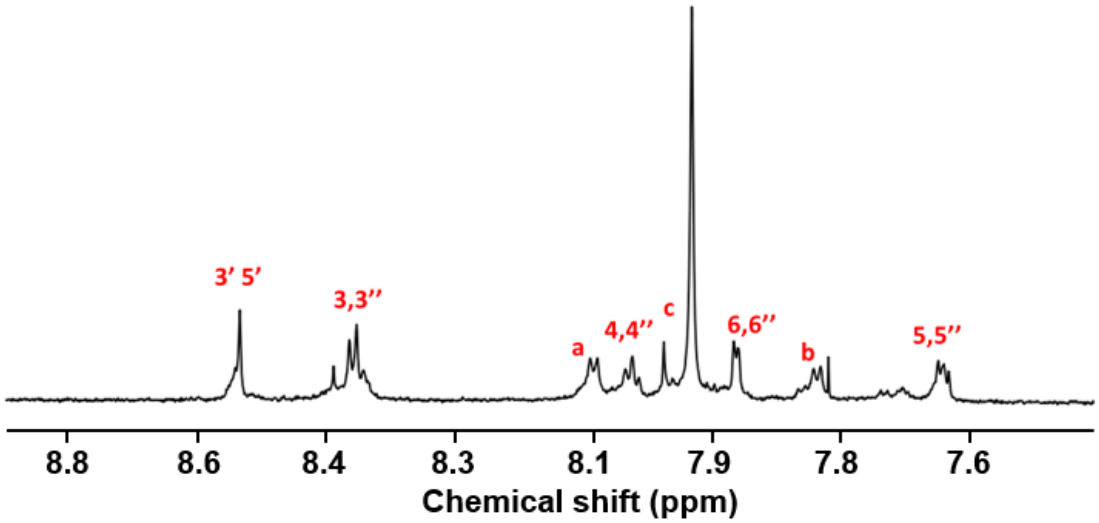

Figure S4. ^{1}H NMR spectrum (400 MHz, 298 K) of **S1** in DMF-d_7 and CD_3CN (1:4, *v/v*).

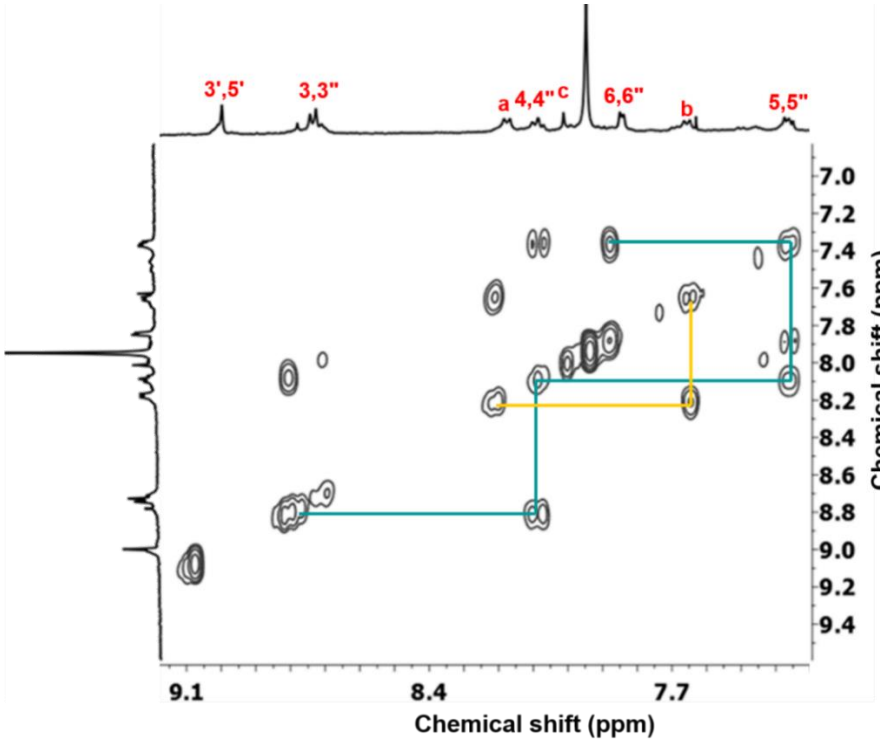

Figure S5. 2D ^{1}H-^{1}H COSY NMR spectrum (500 MHz, 298 K) of **S1** in DMF-d_7 and CD_3CN (1:4, *v*/*v*).

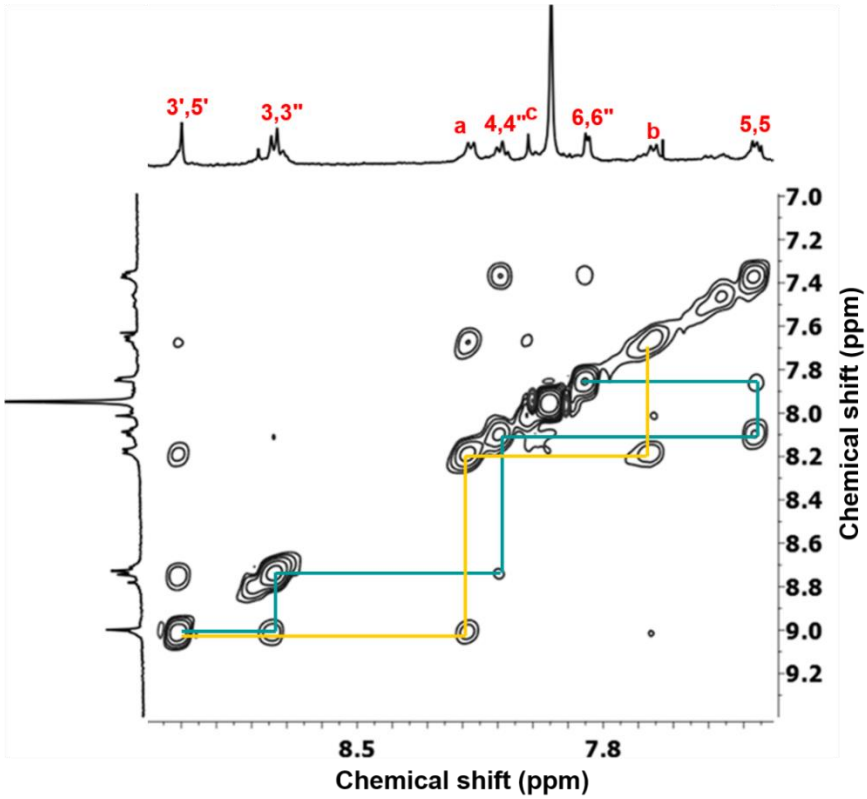

Figure S6. 2D ^{1}H-^{1}H NOESY NMR spectrum (500 MHz, 298 K) of **S1** in DMF-d_7 and CD_3CN (1:4, *v*/*v*).

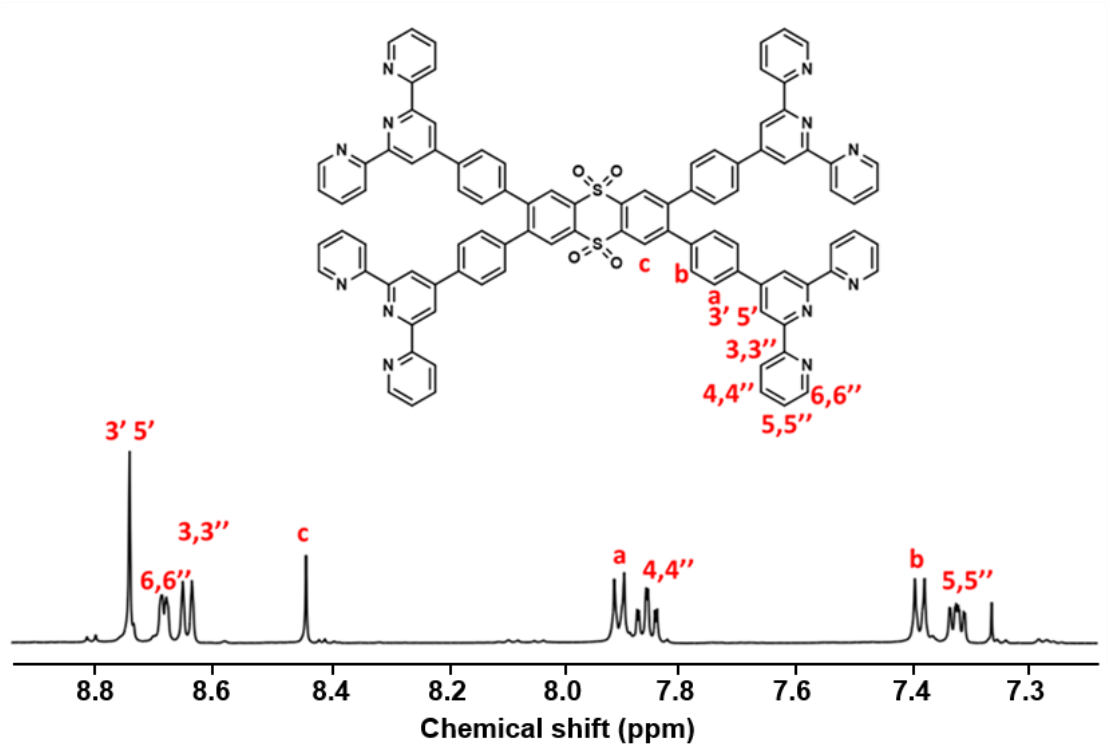

Figure S7. ^{1}H NMR spectrum (500 MHz, 298 K) of **L2** in $CDCl_3$.

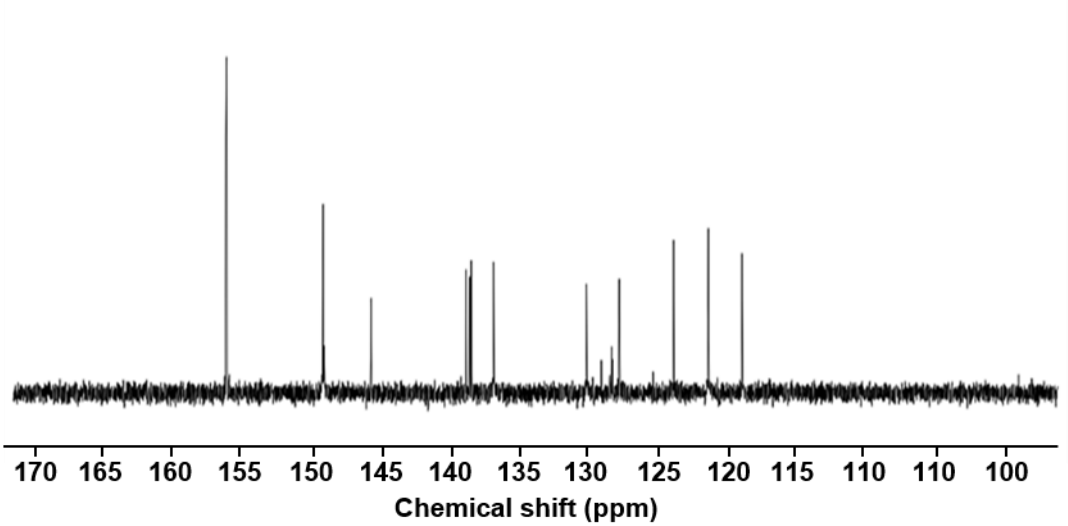

Figure S8. ^{13}C NMR spectrum (125 MHz, 298 K) of **L2** in $CDCl_3$.

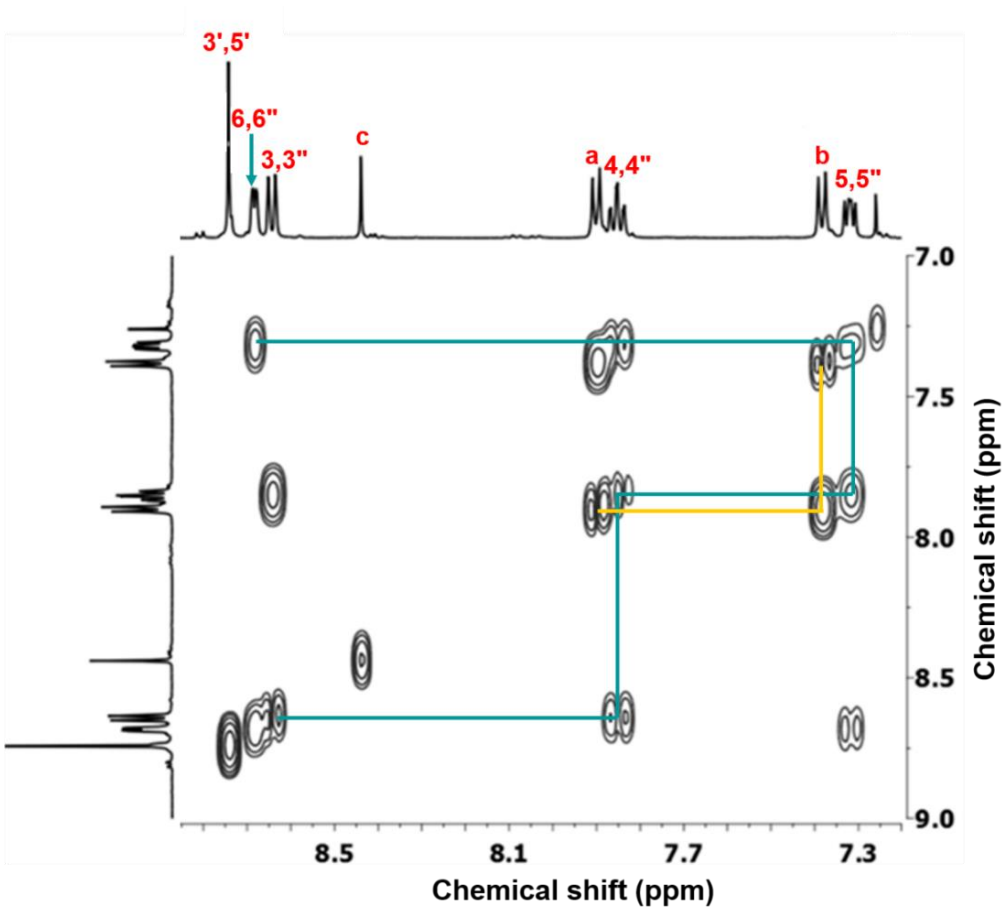

Figure S9. 2D ^{1}H-^{1}H COSY NMR spectrum (500 MHz, 298 K) of **L2** in $CDCl_3$.

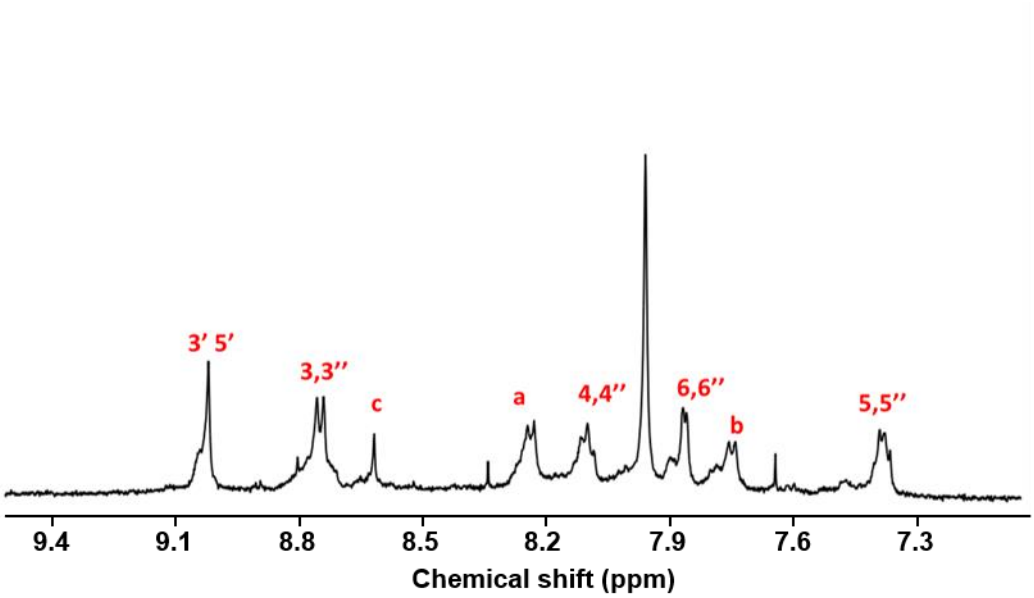

Figure S10. ^{1}H NMR spectrum (400 MHz, 298 K) of **S2** in DMF-d_7 and CD_3CN (1:4, *v/v*).

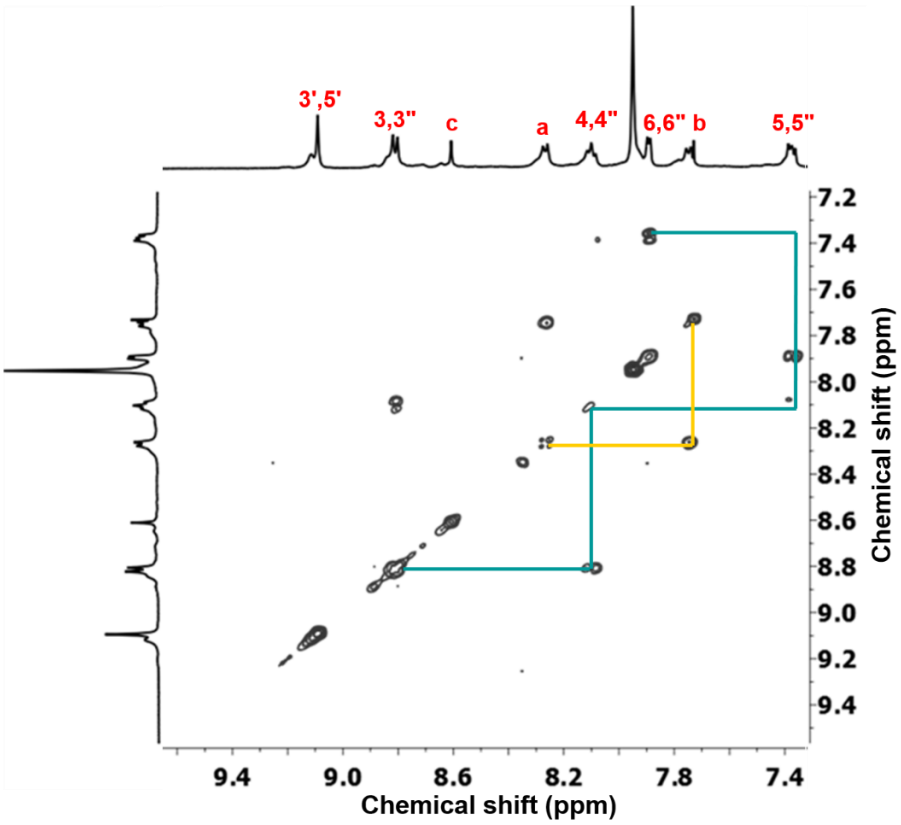

Figure S11. 2D ^{1}H-^{1}H COSY NMR spectrum (500 MHz, 298 K) of **S2** in DMF-d_7 and CD_3CN (1:4, *v*/*v*).

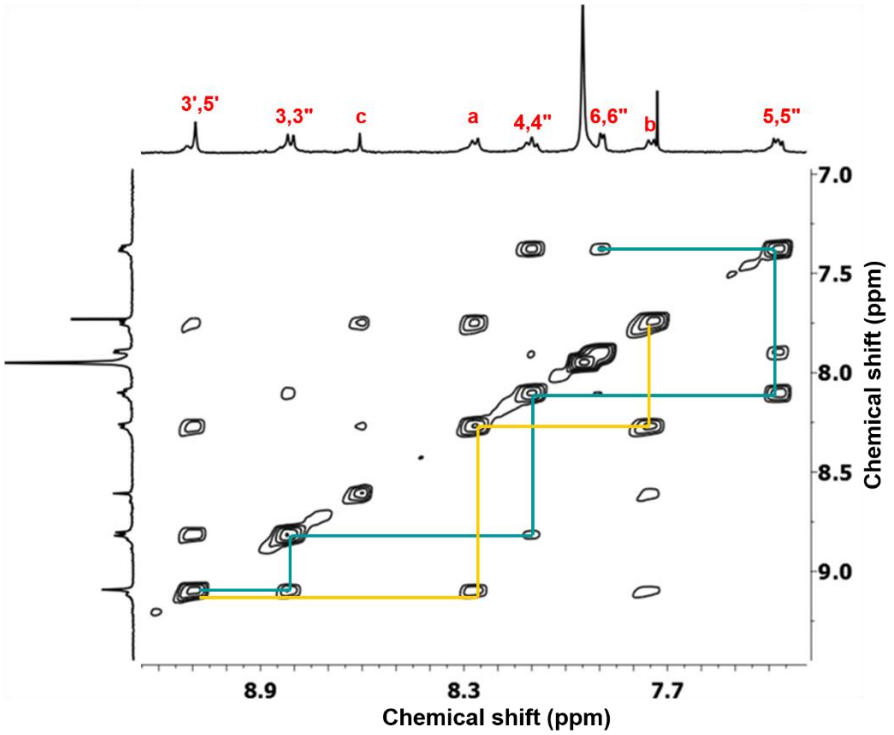

Figure S12. 2D ^{1}H-^{1}H NOESY NMR spectrum (500 MHz, 298 K) of **S2** in DMF-d_7 and CD_3CN (1:4, *v*/*v*).

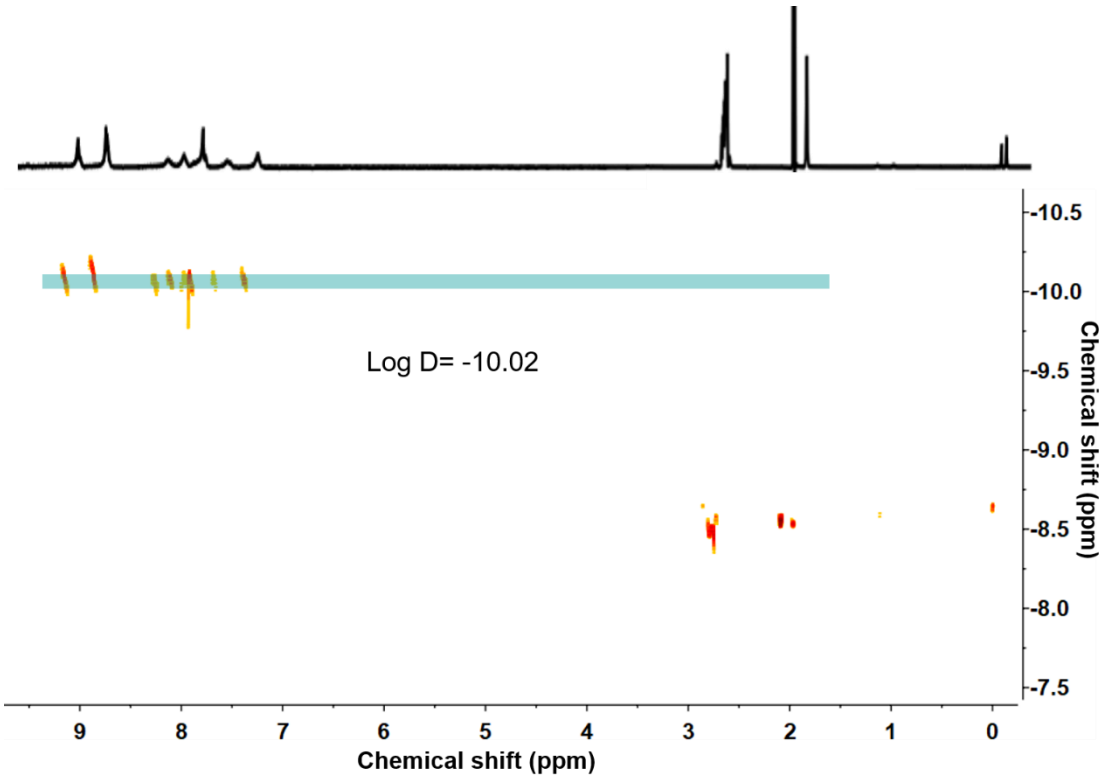

Figure S13. 2D ^{1}H-^{1}H DOSY NMR spectrum of **S1** in DMF-d_7 and CD_3CN (1:4, *v*/*v*).

The sphere hydrodynamic radius can be estimated as follow according to the Stokes-Einstein Equation. Where D is the diffusion constant, k is the Boltzmann's constant, T is the temperature, μ is the viscosity of solvents, and R is the radius of the sphere-like particles:

$$D = \frac{kT}{6\pi\mu R}$$

$D = 10^{-10.02}$ m^2 s^{-1}

$k = 1.38\times10^{-23}$ N m K^{-1}

T = 298 K

$\mu = 4.22\times10^{-4}$ N m^{-2} s (CD_3CN/DMF (4:1, *v*/*v*)[8]

$r = \frac{kT}{6\pi\mu D} = 2.90\times10^{-9}$ m = 2.72 nm

The radius of the spherical **S1** is 5.44 nm, which is consistent with the result of computer modeling.

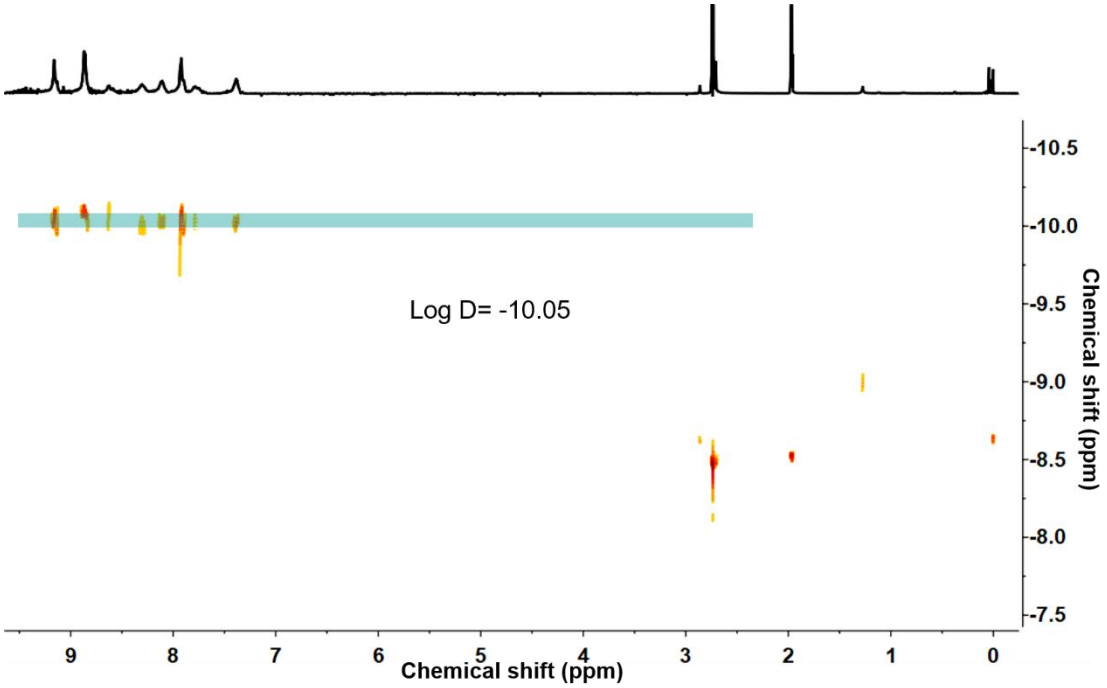

Figure S14. 2D ^{1}H-^{1}H DOSY NMR spectrum of **S2** in DMF-d_7 and CD_3CN (1:4, *v/v*).

The sphere hydrodynamic radius can be estimated as follow according to the Stokes-Einstein Equation. Where D is the diffusion constant, k is the Boltzmann's constant, T is the temperature, μ is the viscosity of solvents, and R is the radius of the sphere-like particles:

$$D = \frac{kT}{6\pi\mu R}$$

$D = 10^{-10.05}$ m^2 s^{-1}

$k = 1.38\times10^{-23}$ N m K^{-1}

T = 298 K

$\mu = 4.22\times10^{-4}$ N m^{-2} s (CD_3CN/DMF (4:1, *v/v*)[8]

$r = \frac{kT}{6\pi\mu D} = 2.90\times10^{-9}$ m = 2.91 nm

The radius of the spherical **S2** is 5.82 nm, which is consistent with the result of computer modeling.

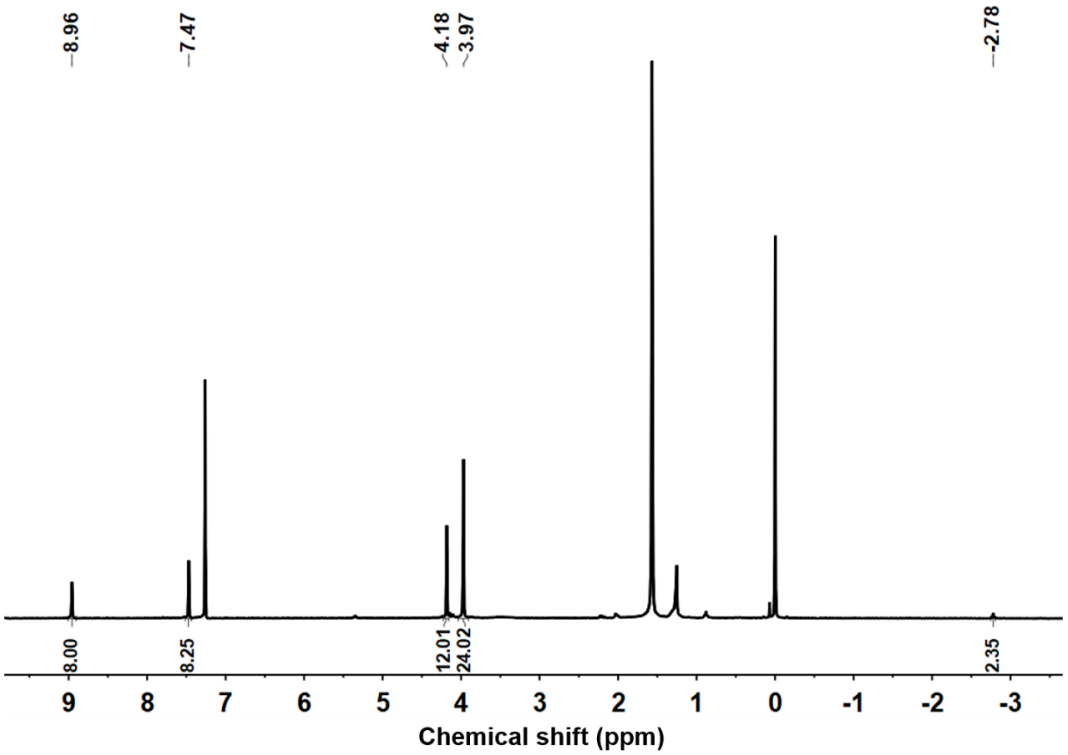

Figure **S15**. ^{1}H NMR spectrum (400 MHz, 298 K) of 5,10,15,20-tetrakis(3,4,5-trimethoxyphenyl) porphyrin in DMSO-d_6.

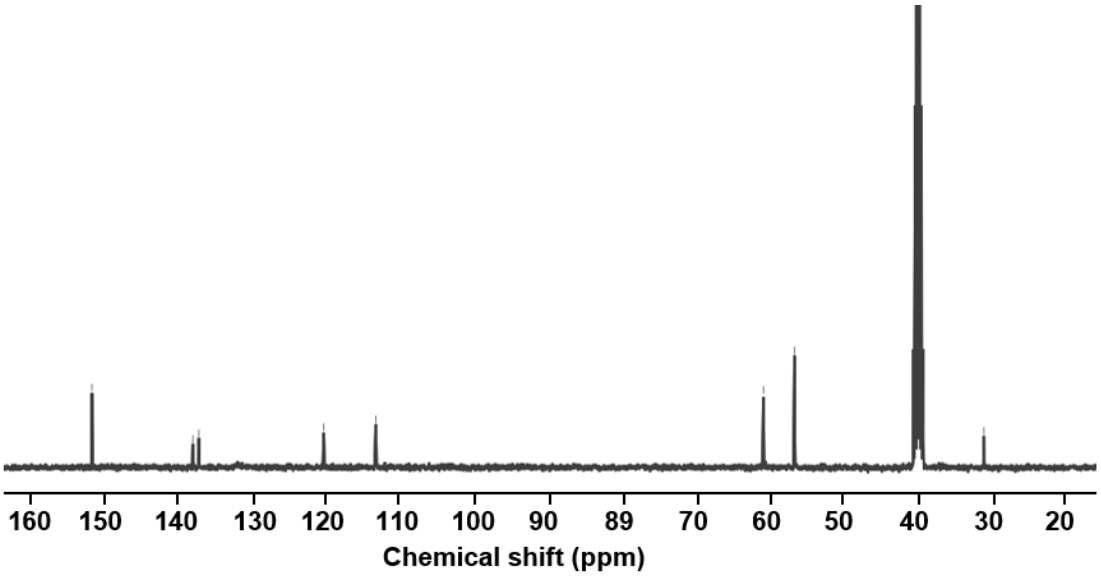

Figure S16. ^{13}C NMR spectrum (100 MHz, 298 K) of 5,10,15,20-tetrakis(3,4,5-trimethoxyphenyl) porphyrin in DMSO-d_6.

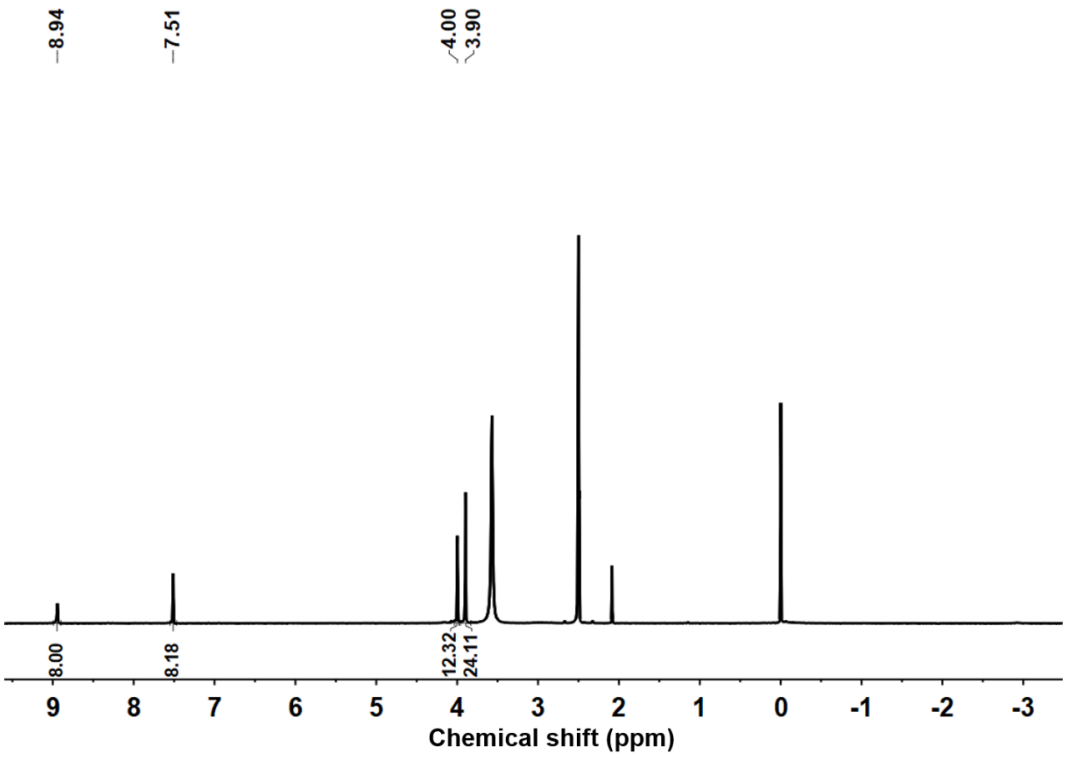

Figure S17. ^{1}H NMR spectrum (400 MHz, 298 K) of 5,10,15,20-tetrakis(3,4,5-trimethoxyphenyl) porphyrin zinc in DMSO-d_6.

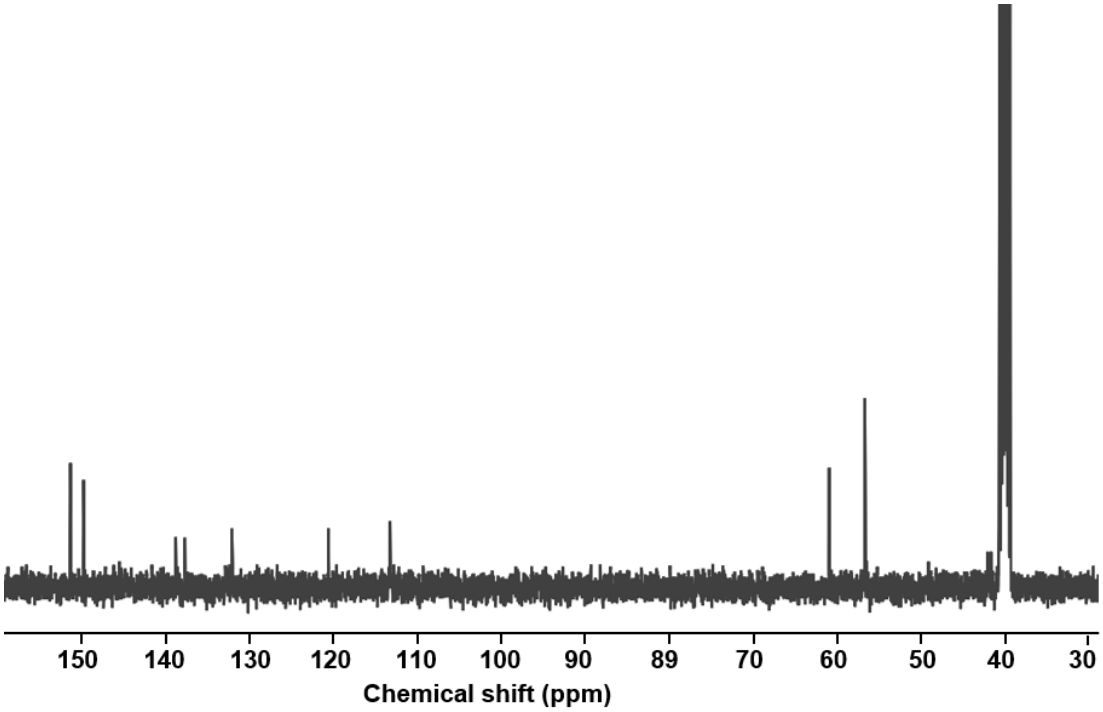

Figure S18. ^{13}C NMR spectrum (100 MHz, 298 K) of 5,10,15,20-tetrakis(3,4,5-trimethoxyphenyl) zinc porphyrin in DMSO-d_6.

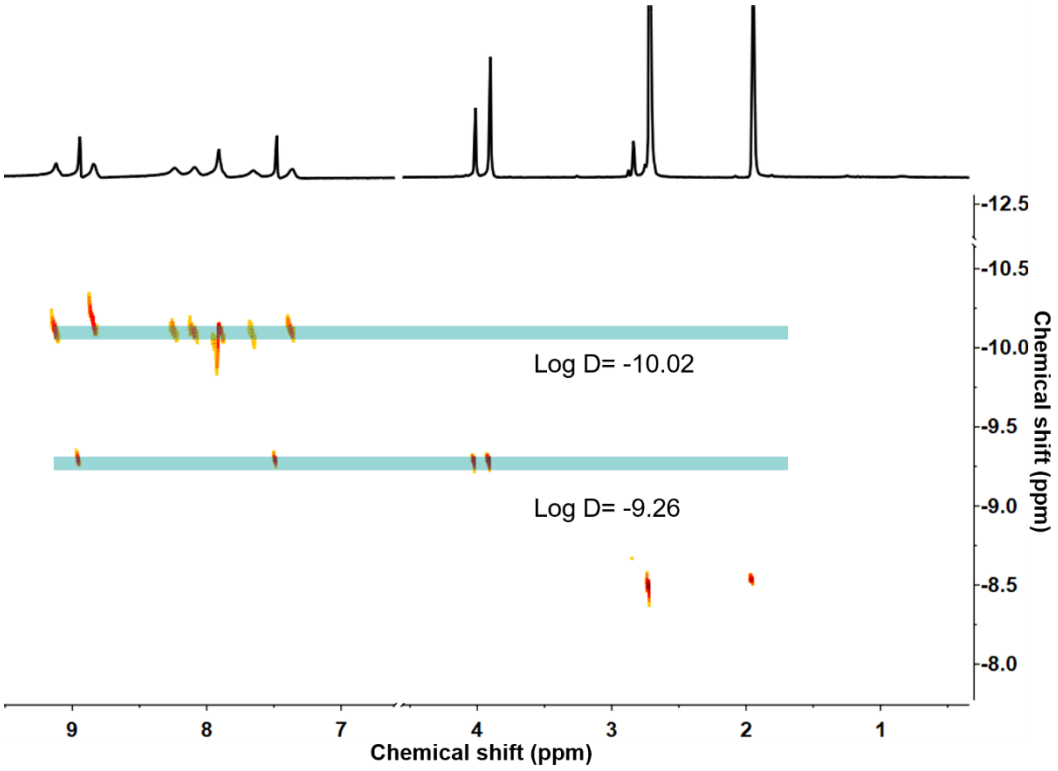

Figure S19. 2D ^{1}H-^{1}H DOSY NMR spectrum of **S1** combing zinc porphyrin in DMF-d_7 and CD_3CN (1:4, *v*/*v*).

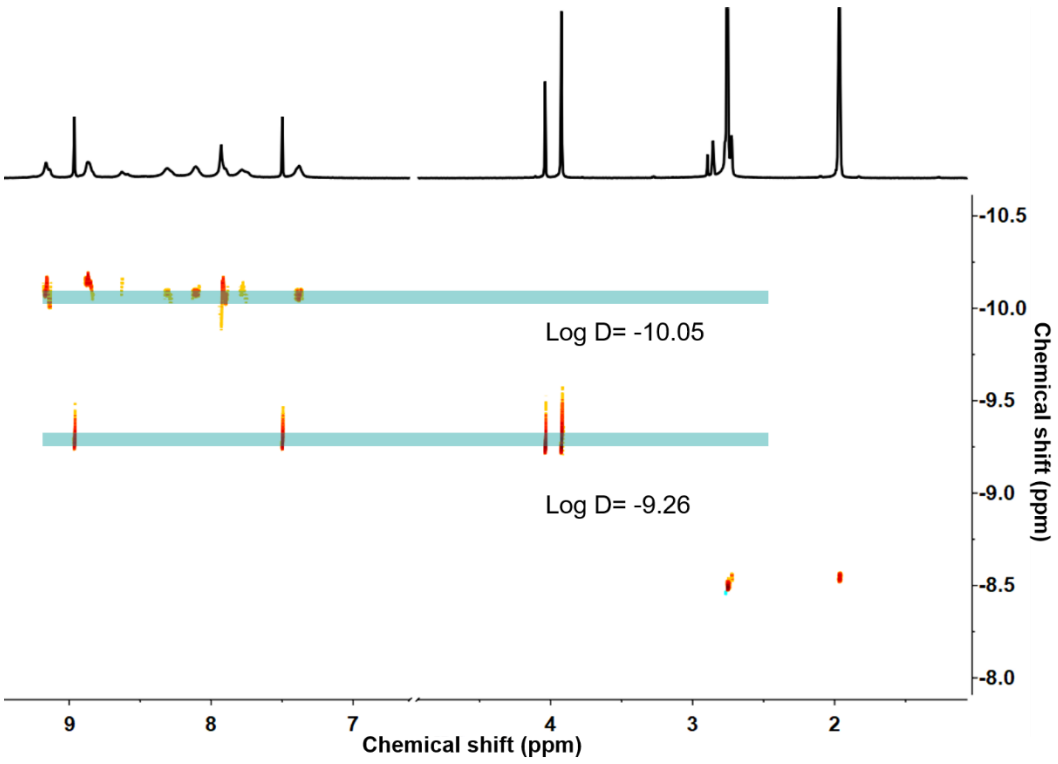

Figure S20. 2D ^{1}H-^{1}H DOSY NMR spectrum of **S2** combing zinc porphyrin in DMF-d_7 and CD_3CN (1:4, *v*/*v*).

6. ESI-MS spectra data of supramolecules (NTf_2^- as counterion)

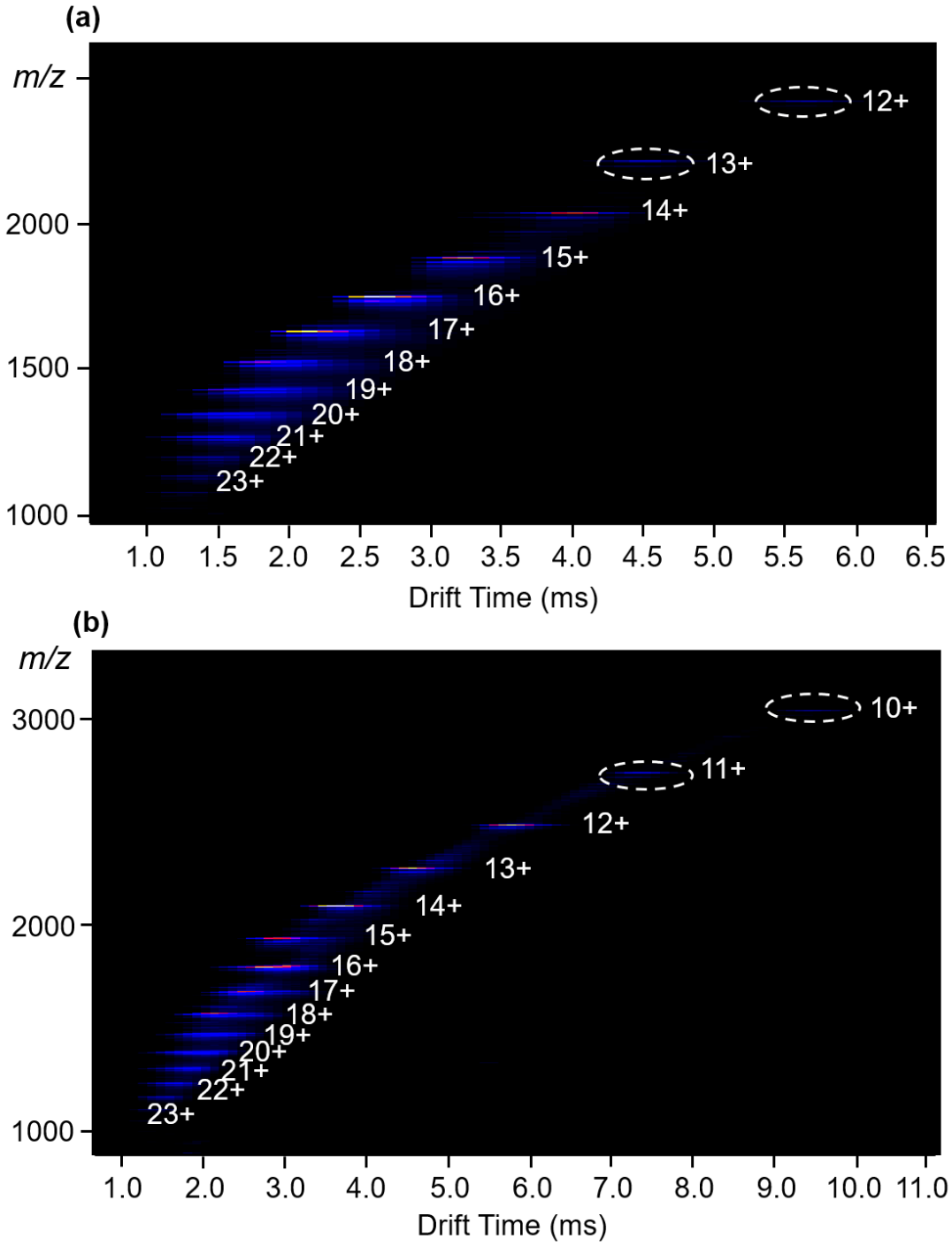

Figure S21. TWIM-MS plot (*m/z* vs drift time) of **S1** (a) and **S2** (b).

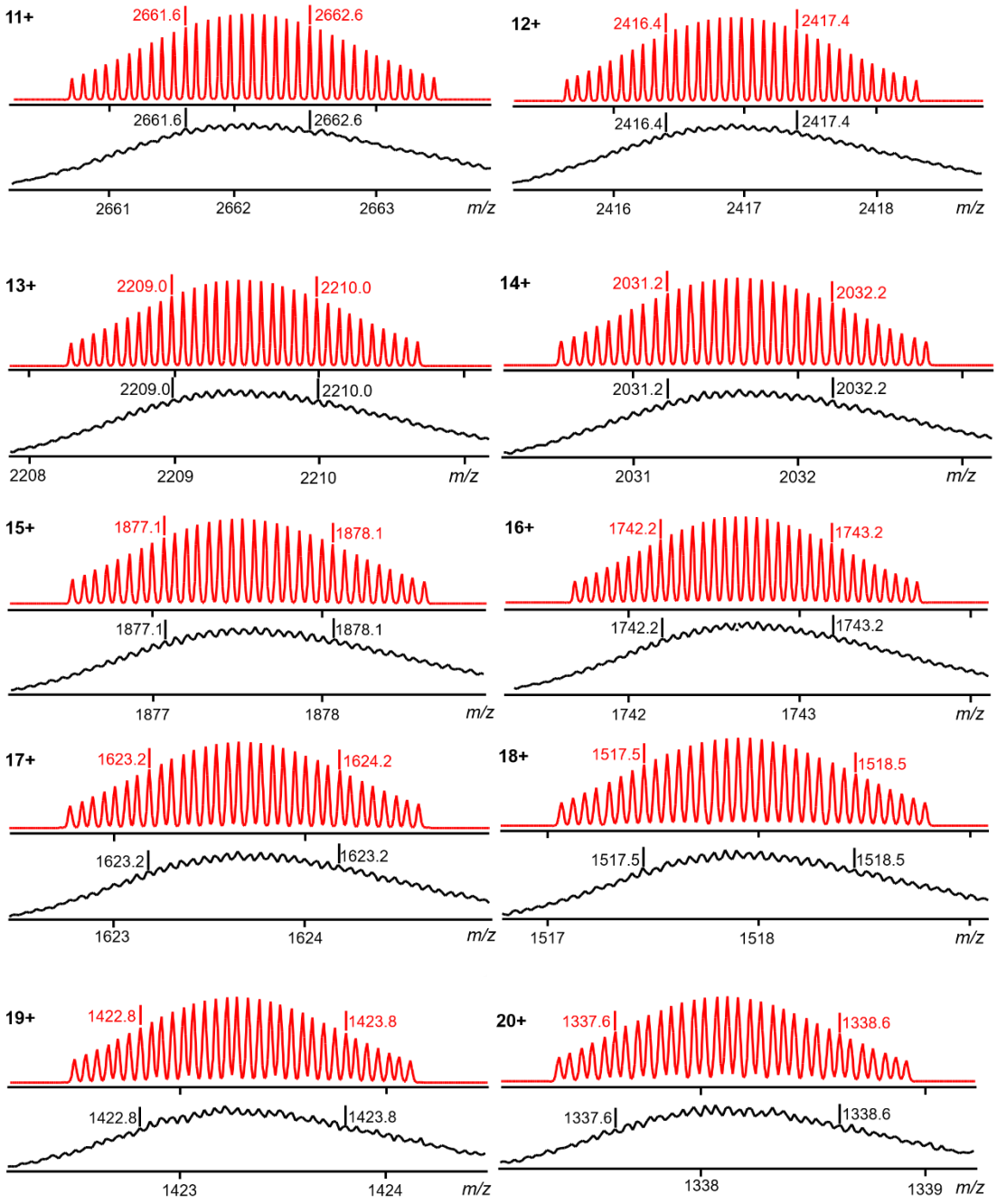

Figure S22. Measured (bottom) and calculated (top) isotope patterns for different charge states observed from **S1** (NTf_2^- as counterion).

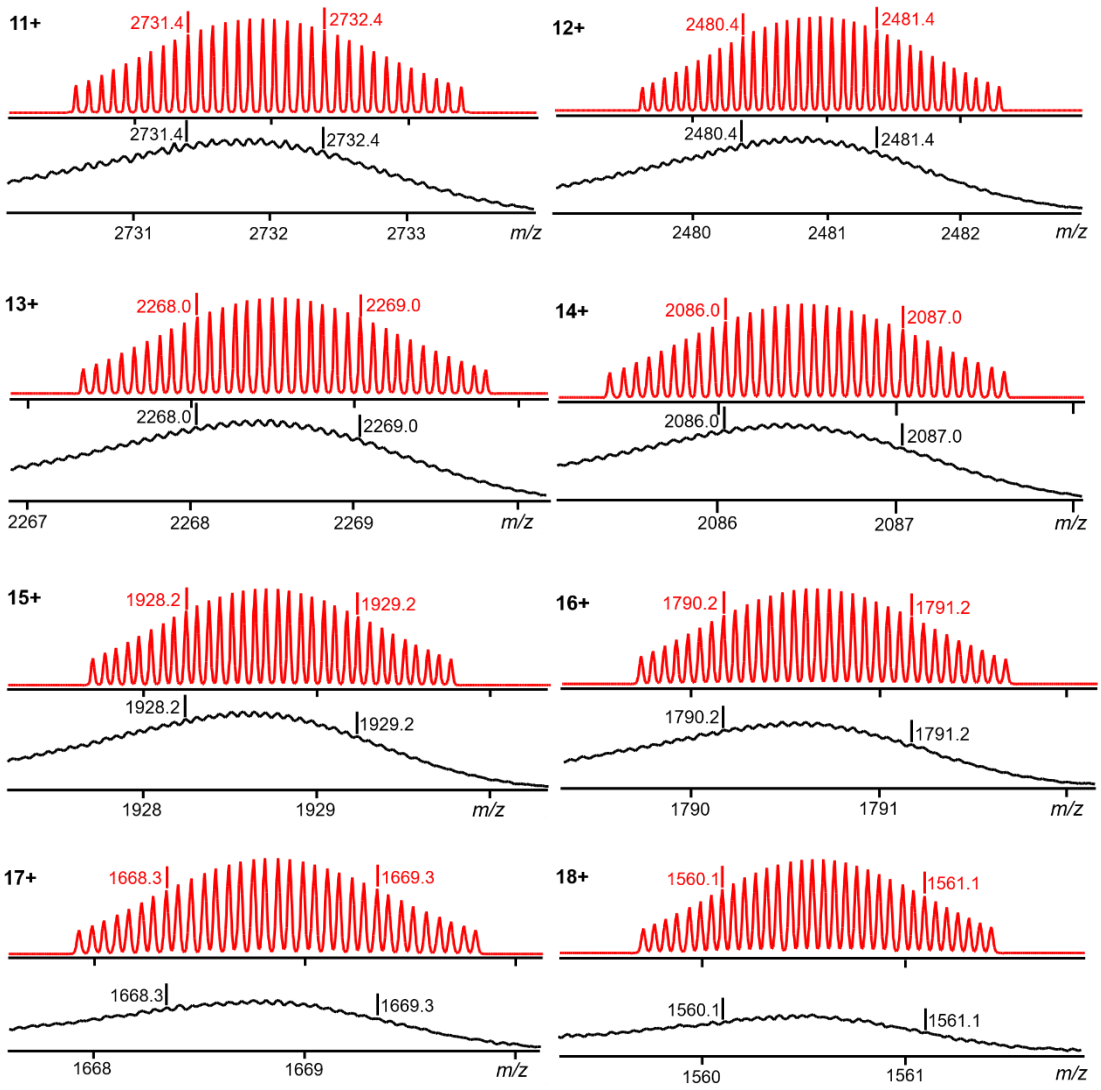

Figure S23. Measured (bottom) and calculated (top) isotope patterns for different charge states observed from **S2** (NTf_2^- as counterion).

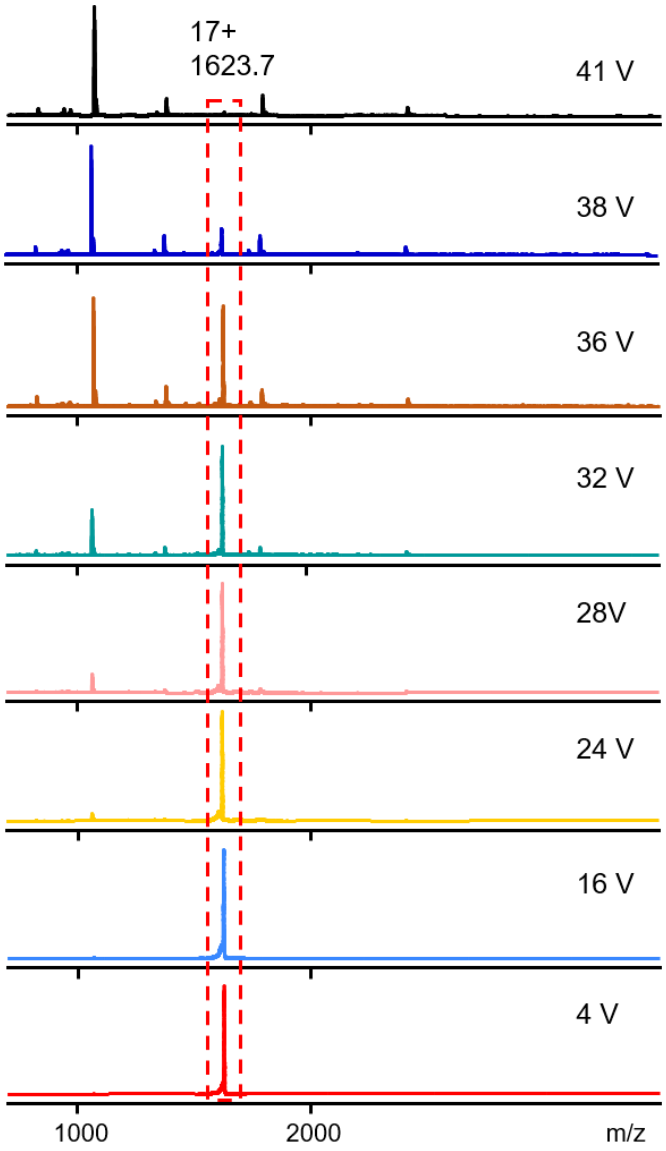

Figure S24. gMS^2 of **S1** at *m/z* 1623.7 with different collision energies.

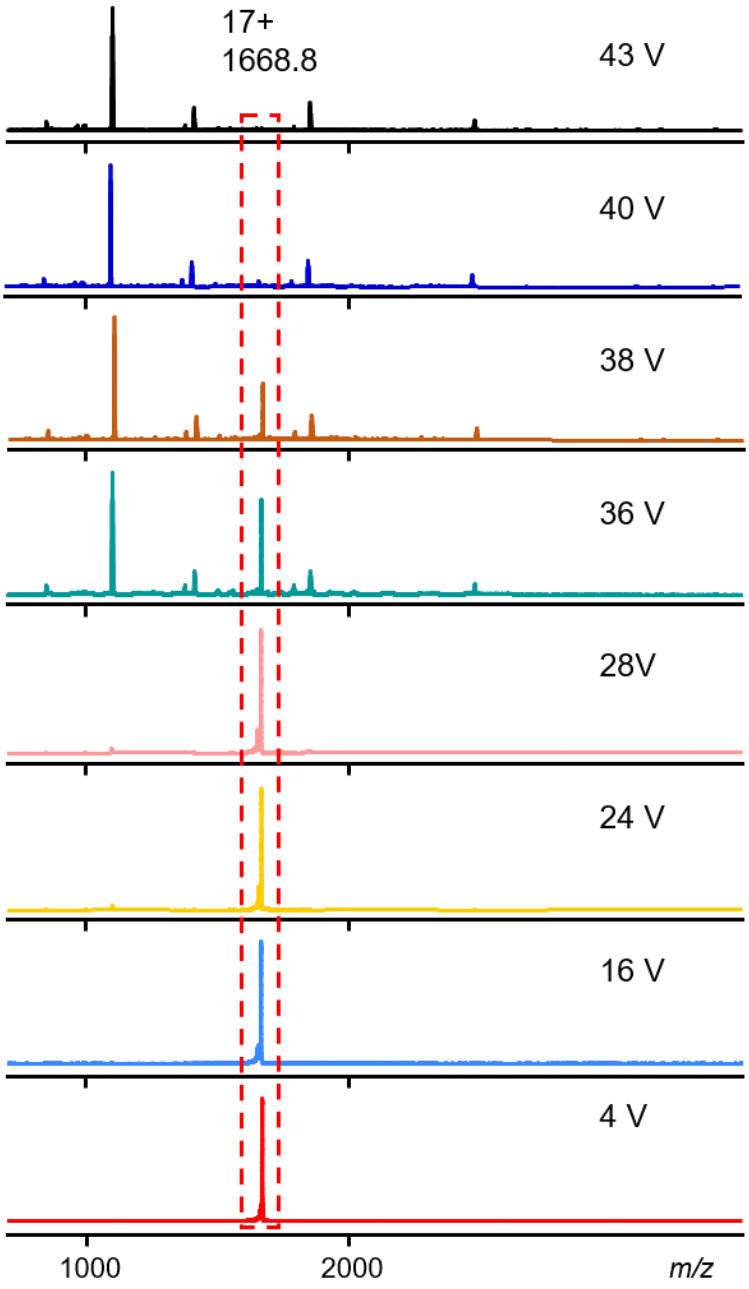

Figure S25. gMS^2 of **S2** at *m/z* 1668.8 with different collision energies.

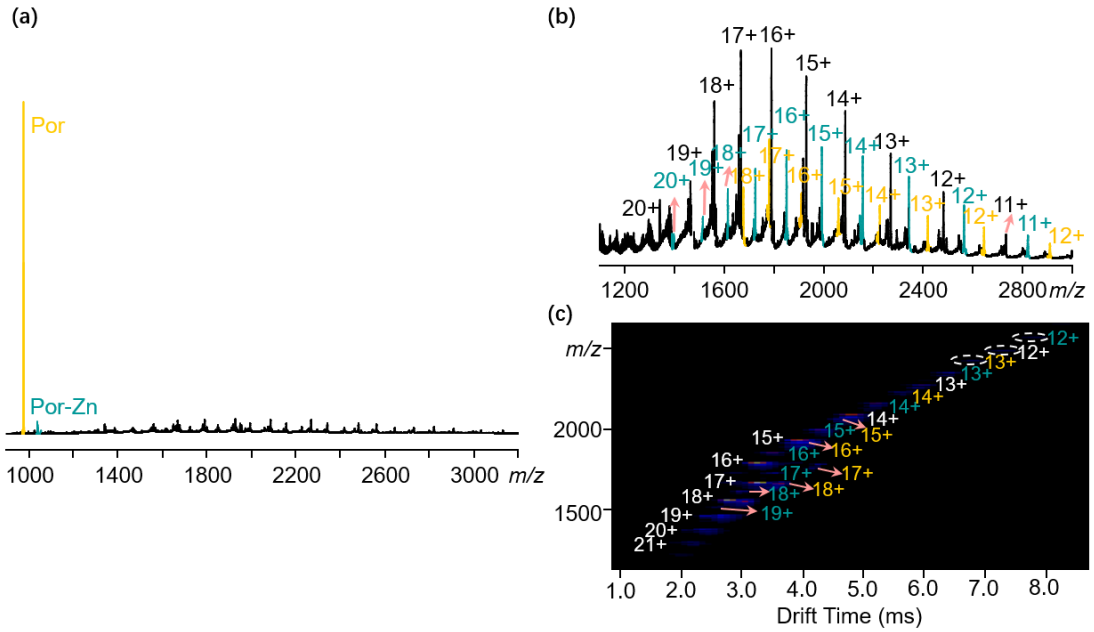

Figure S26. (a) ESI-MS (full spectra) of one porphyrin adducts **S1 ⊃ G**, (b) ESI-MS of free **S1** (black), one zinc porphyrin adducts **S1 ⊃ G** (green), two zinc porphyrin adducts **S1 ⊃ G$_2$** (yellow), (c) TWIM-MS of free **S1** (black), one zinc porphyrin adducts **S1 ⊃ G** (green), two zinc porphyrin adducts **S1 ⊃ G$_2$** (yellow).

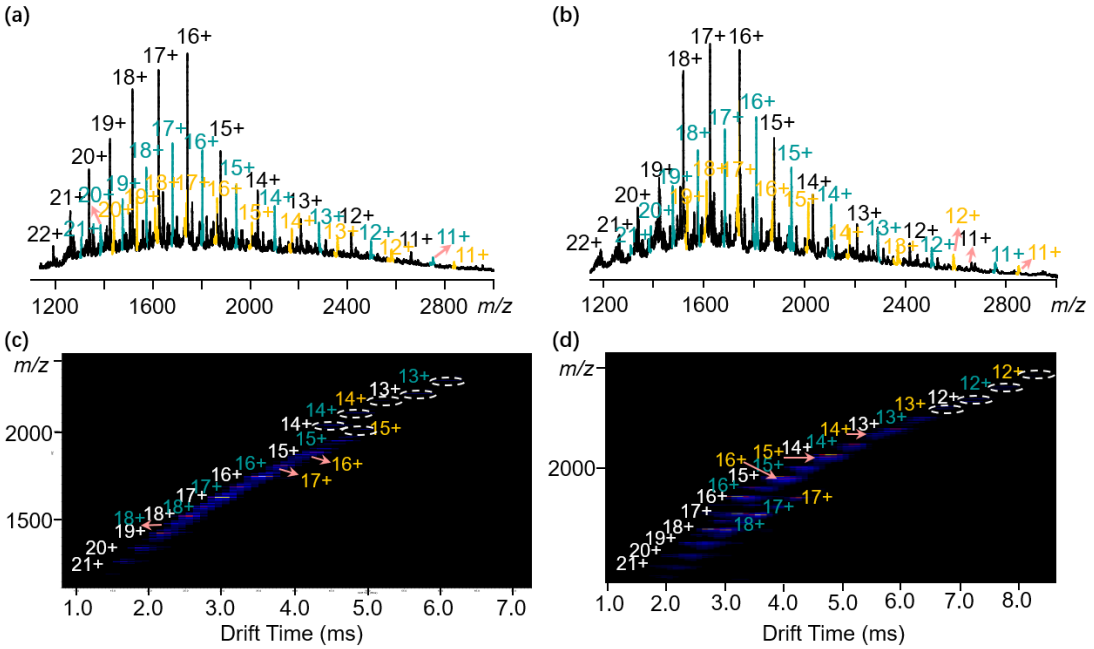

Figure S27. (a) (b) ESI-MS of free **S1 (S2)** (black), one porphyrin adducts **S1 (S2) ⊃ G** (green), two porphyrin adducts **S1 (S2) ⊃ G$_2$** (yellow), (c) (d) TWIM-MS of free **S1 (S2)** (black), one porphyrin adducts **S1 (S2) ⊃ G** (green), two porphyrin adducts **S1 (S2) ⊃ G$_2$** (yellow).

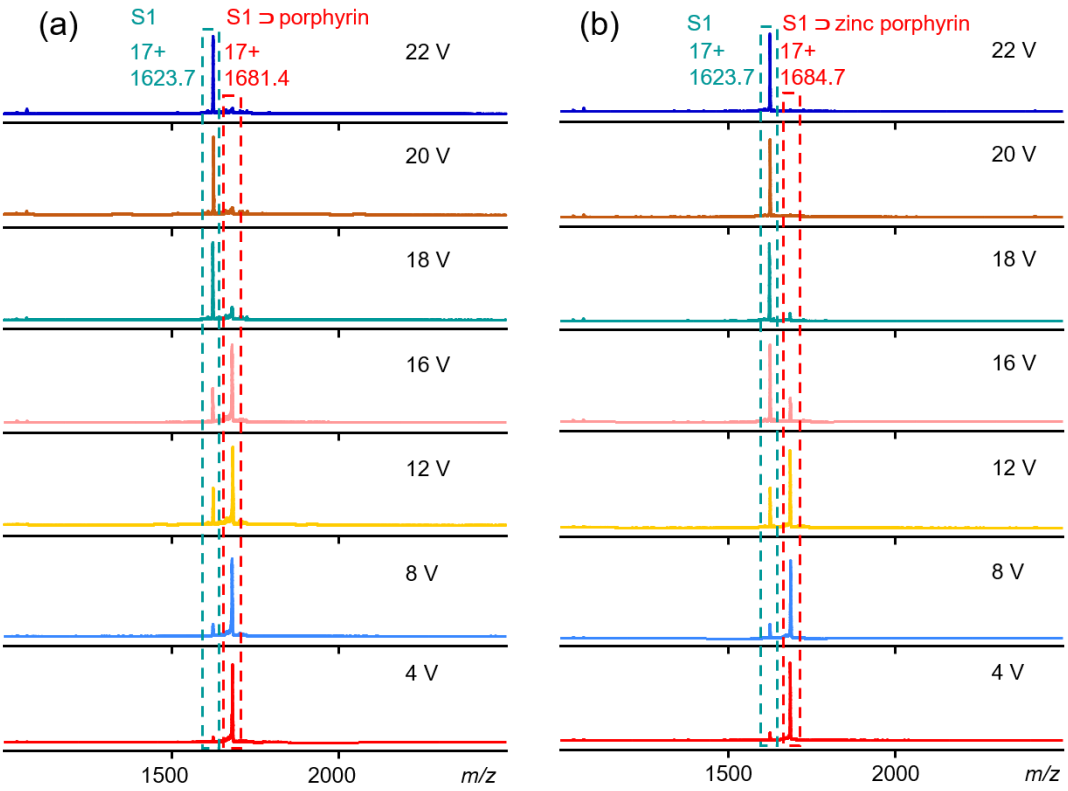

Figure S28. (a) gMS^2 of one porphyrin adducts **S1 ⊃ G** (NTf_2^-) at *m/z* 1681.4 with different collision energies; (b) gMS^2 of one zinc porphyrin adducts **S1 ⊃ G** (NTf_2^-) at *m/z* 1684.7 with different collision energies.

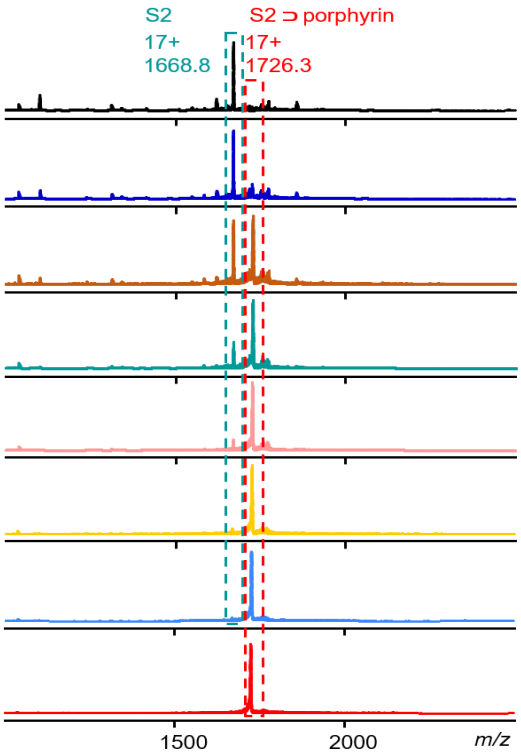

Figure S29. gMS^2 of one porphyrin adducts **S2 ⊃ G** (NTf_2^-) at *m/z* 1726.3 with different collision energies.

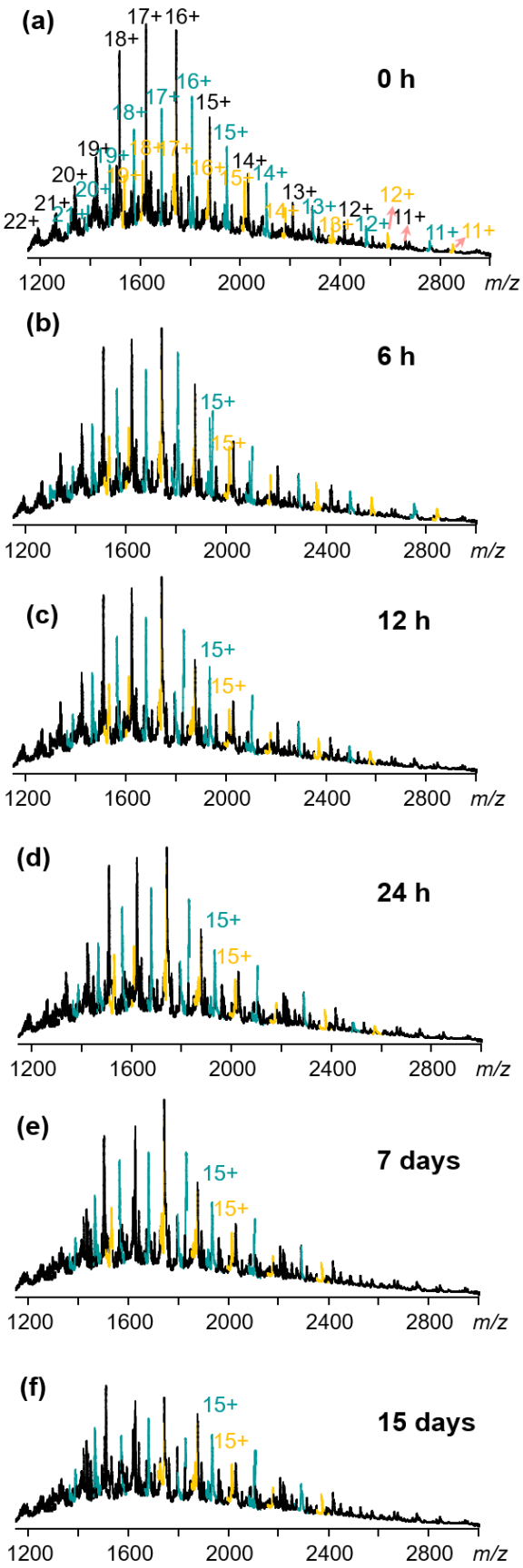

Figure S30. (a) ESI-MS of porphyrin adducts of **S1** with different times. (a) 0 h, (b) 6 h, (c) 12 h, (d) 24 h (e) 7 days, (f) 15 days.

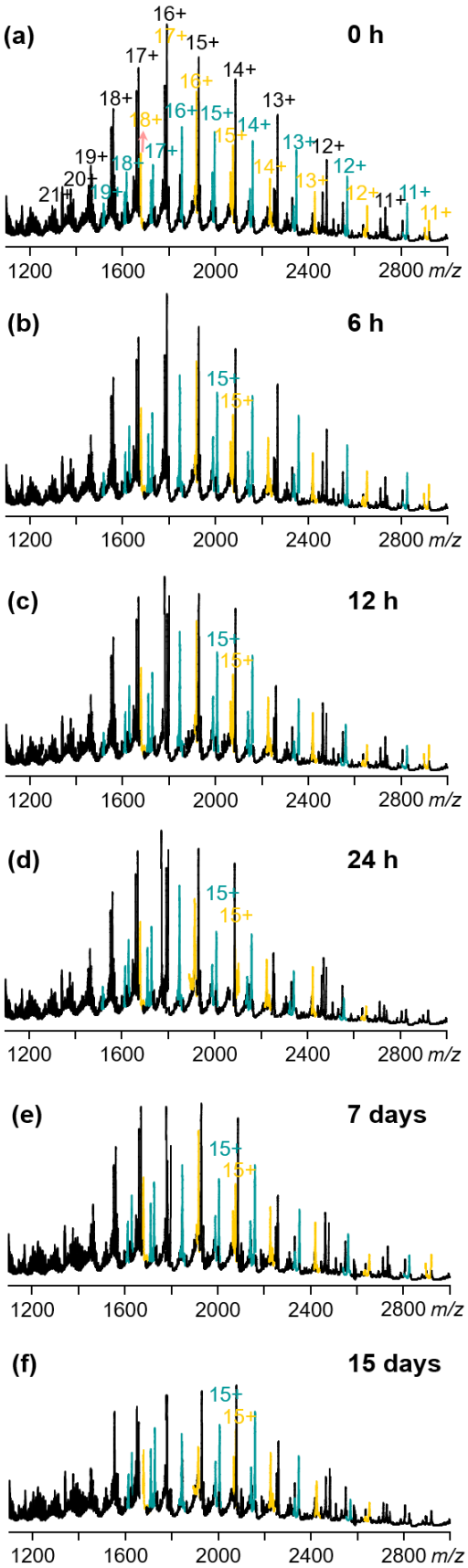

Figure S31. (a) ESI-MS of porphyrin adducts of **S2** with different times. (a) 0 h, (b) 6 h, (c) 12 h, (d) 24 h (e) 7 days, (f) 15 days.

7. TEM images of supramolecules (NTf_2^- as counterion)

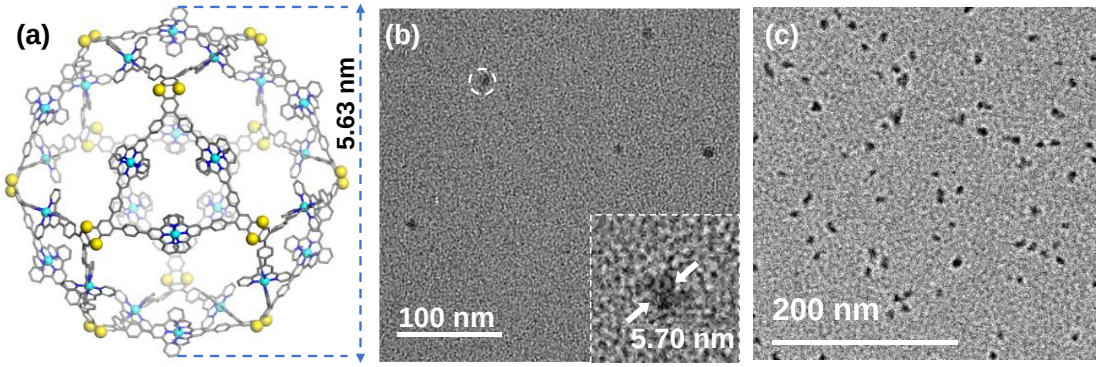

Figure S32. TEM images of **S1** on the lacey carbon coated Cu grid**.**

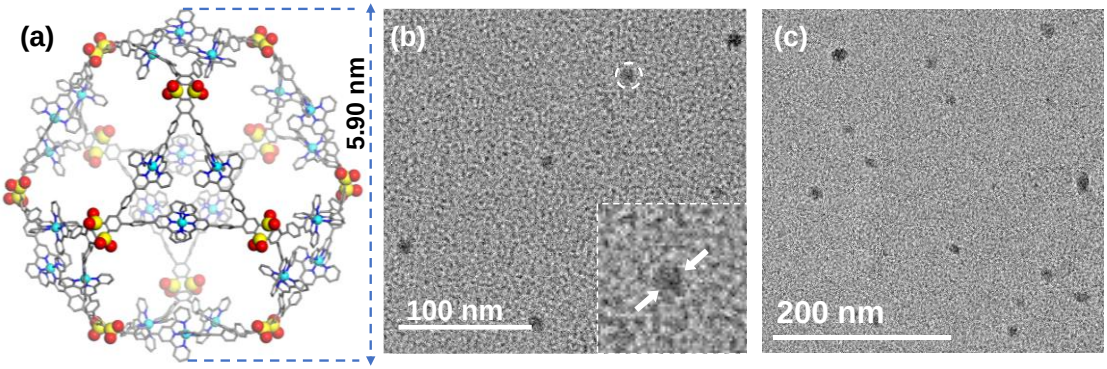

Figure S33. TEM images of **S2** on the lacey carbon coated Cu grid.

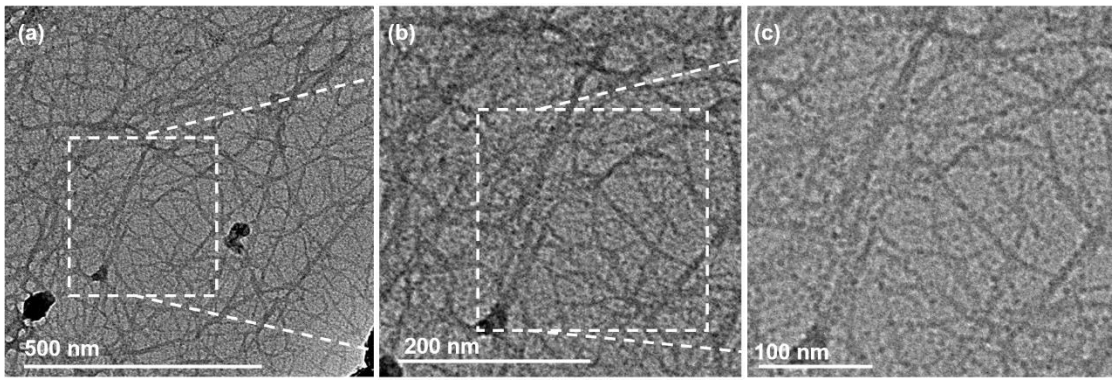

Figure S34. TEM images of nanofibers assembled by **S1**.

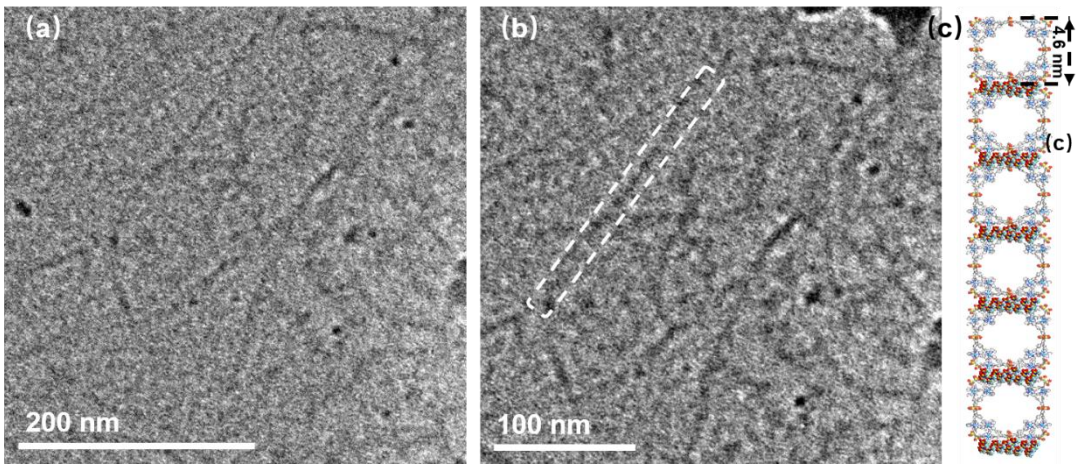

Figure S35. (a) (b) TEM images of nanofibers assembled by **S2** (2 mg/ml in DMF solution under ethyl ether vapor); (c) the probable stacking approaches of **S2** (stacking with square surfaces as contact surfaces).

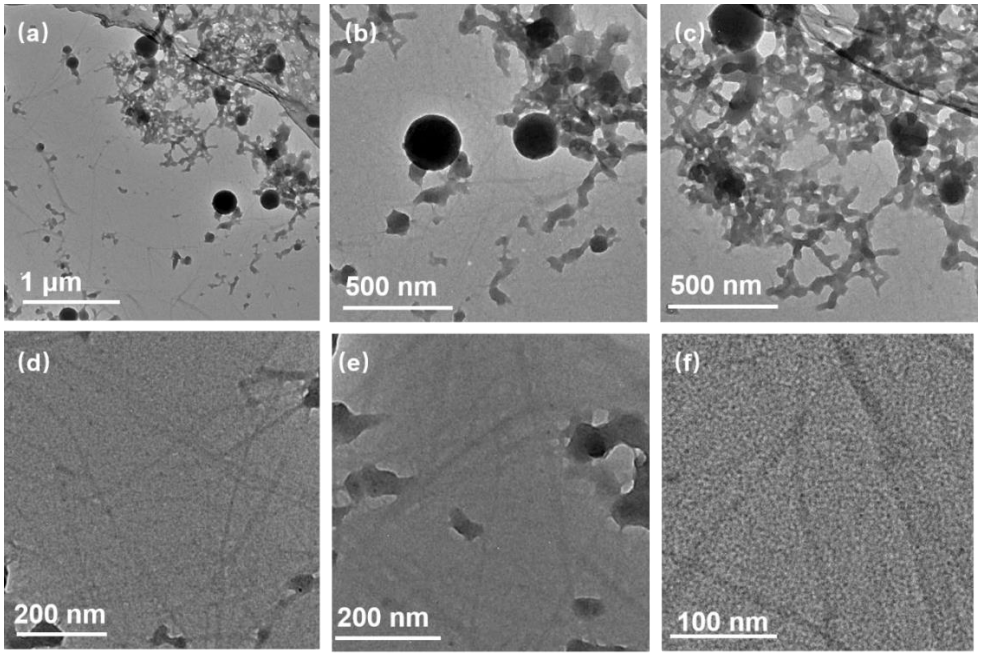

Figure S36. The TEM images of the same **S2** sample captured under different areas, which may reveal the possible growing processes of the nanofibers for **S2**.

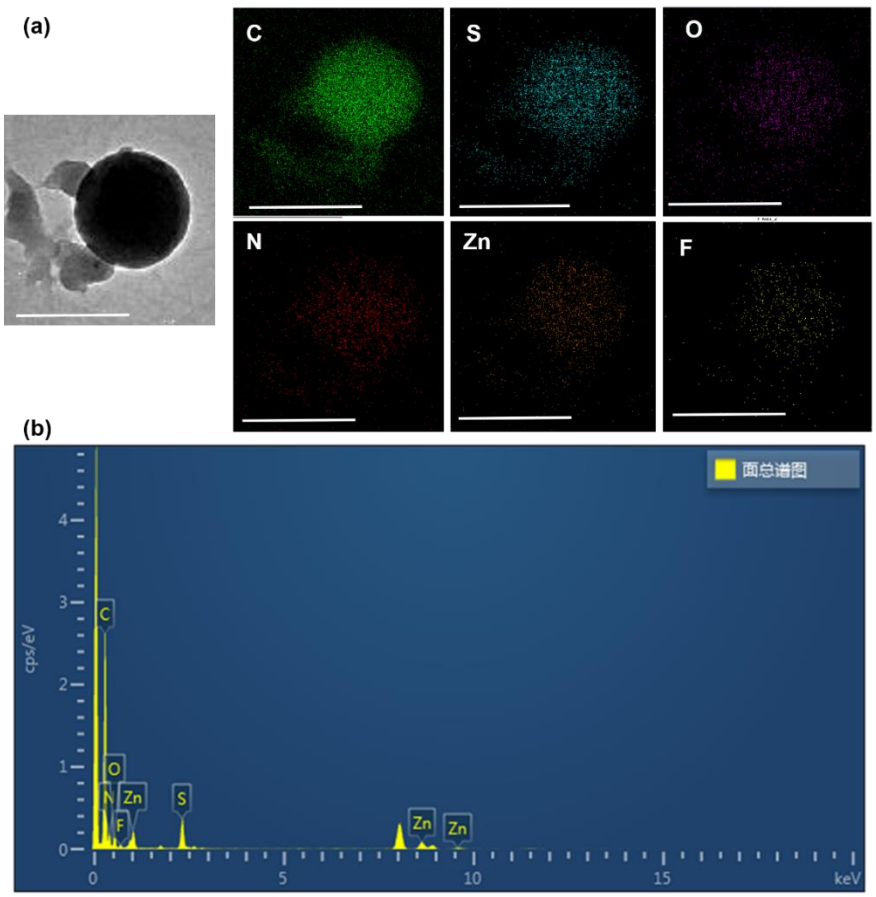

Figure S37. (a) Element mapping of selected areas. (b) TEM-EDX spectrum of the nanowires of **S2** collected on a lacey carbon covered Cu grid.[9]

Table S1. Atomic ratios of the elements in the nanowires of **S2** collected on a lacey carbon covered Cu grid by TEM-EDS

element	k	Absorption correction	wt%	wt% Sigma	Element analysis %
C	2.74533	1.00	80.10	0.52	46.32
N	3.46969	1.00	4.57	0.48	8.31
O	2.00298	1.00	4.61	0.22	9.49
F	1.70760	1.00	0.79	0.12	16.91
S	0.99241	1.00	6.64	0.17	11.89
Zn	1.32169	1.00	3.28	0.15	7.08
Total amount:			100.00		

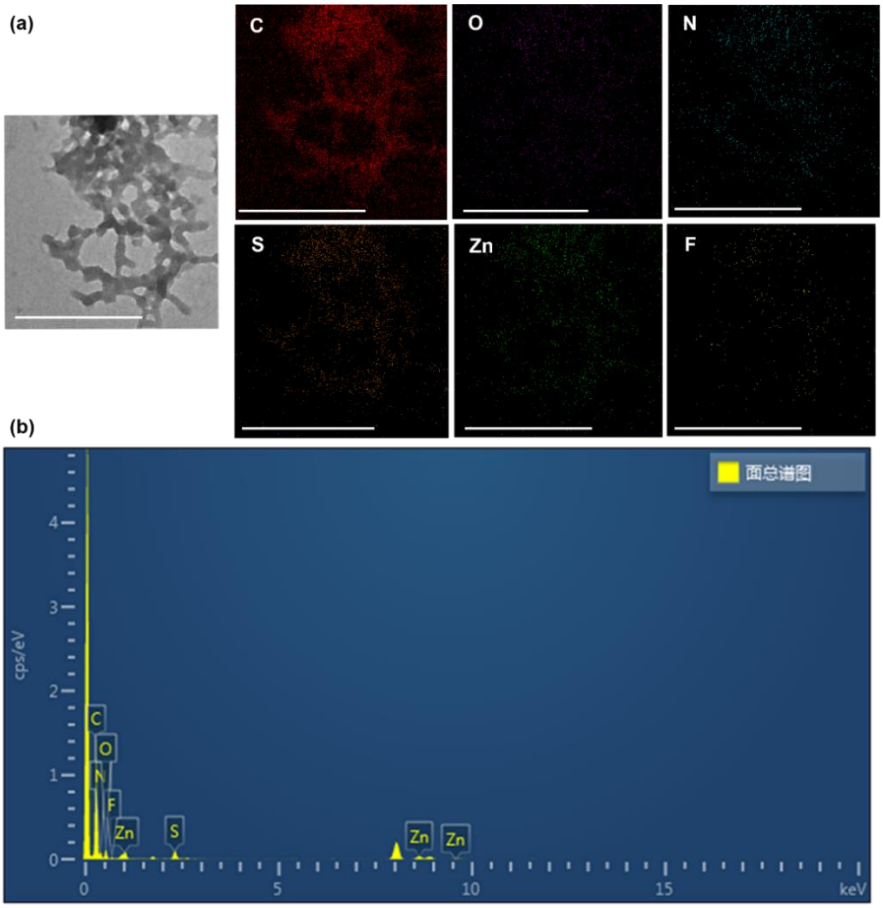

Figure S38. (a) Element mapping of selected areas. (b) TEM-EDX spectrum of the transferred nanowires collected on a lacey carbon covered Cu grid.

Table S2. Atomic ratios of the elements in the nanowires of **S2** collected on a lacey carbon covered Cu grid by TEM-EDS

element	k	Absorption correction	wt%	wt% Sigma	Element analysis %
C	2.74533	1.00	84.95	0.50	45.24
N	3.46969	1.00	3.40	0.46	8.12
O	2.00298	1.00	5.09	0.21	11.59
F	1.70760	1.00	0.56	0.10	16.51
S	0.99241	1.00	3.36	0.12	11.61
Zn	1.32169	1.00	2.64	0.13	6.93
Total amount:			100.00		

8. Fluorescence emission measurement

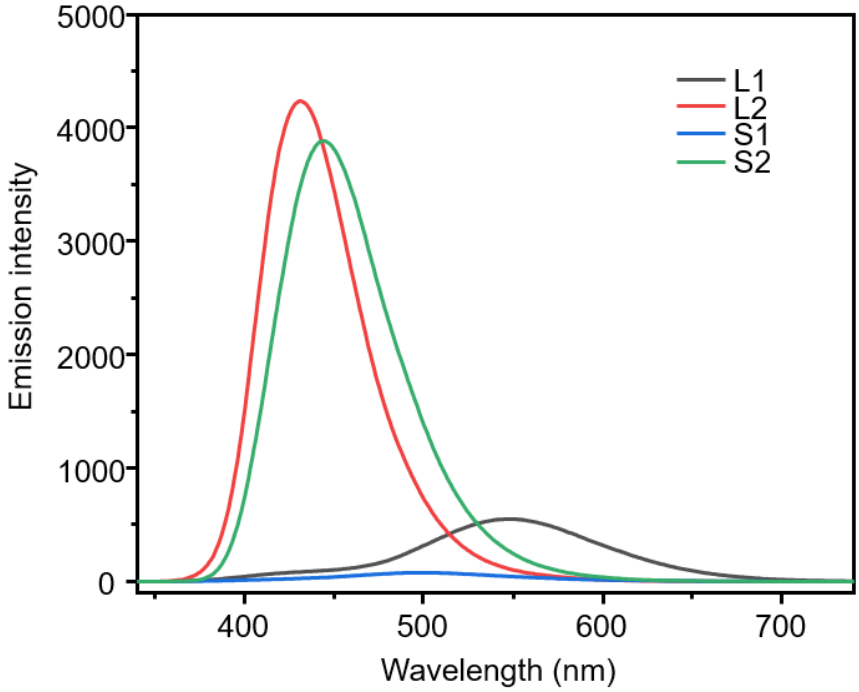

Figure S39. Fluorescence spectrum (λ_{ex} = 340 nm, c = 1.0 μM) of ligands **L1**, **L2** and complexs **S1**, **S2**.

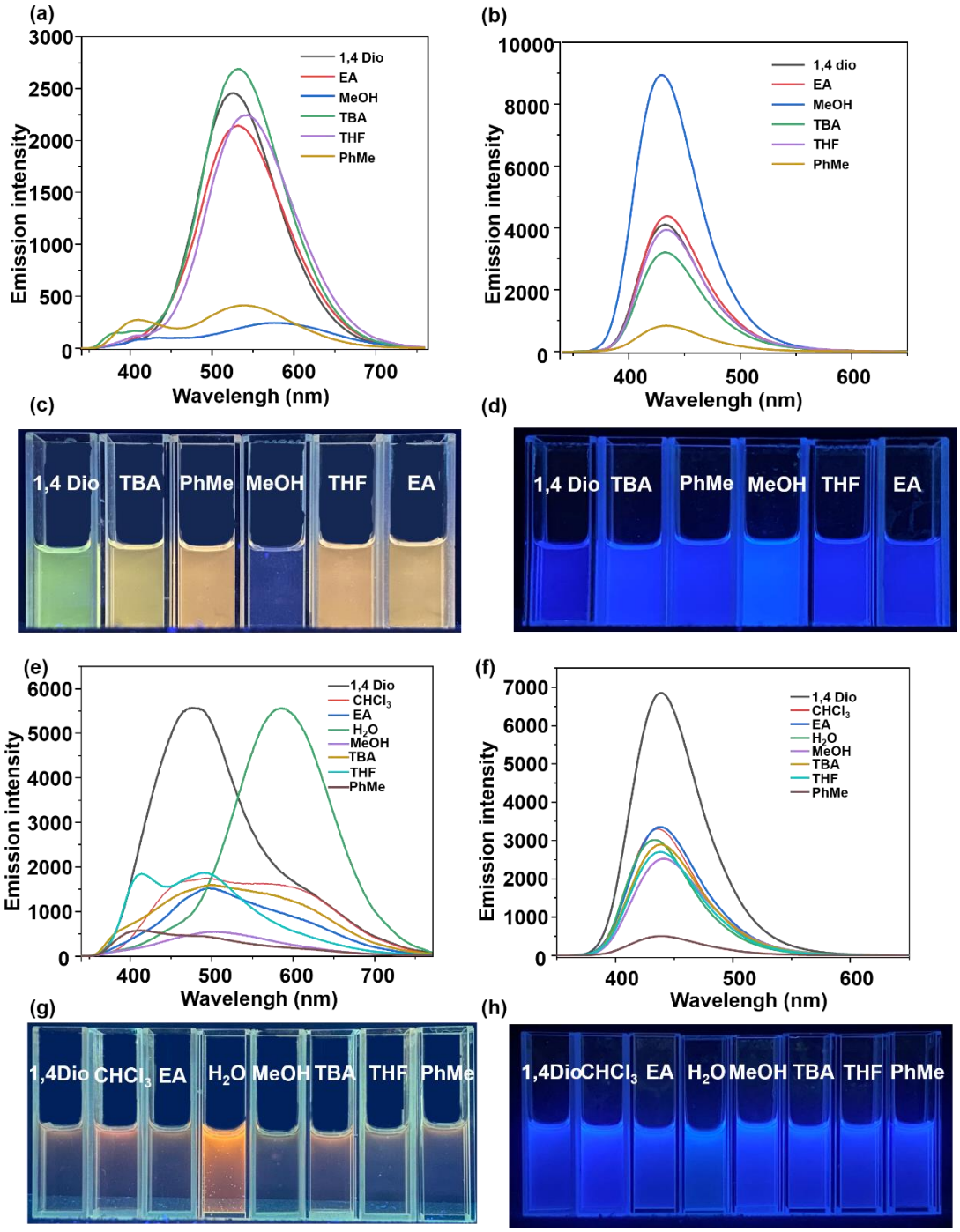

Figure S40. (a) (b) Fluorescence spectrum of **L1** and **L2** in different poor solvents (60%) (λ_{ex} = 340 nm, c = 1.0 μM) (1,4 dioxane, ethyl acetate, methanol, tert-butanol, tetrahydrofuran, toluene); (c) (d) Photographs of florescence changes of **L1** and **L2**; (e) (f) Fluorescence spectrum of **S1** and **S2** in different poor solvents (60%) (λ_{ex} = 340 nm, c = 1.0 μM) (1,4 dioxane, chloromethane, ethyl acetate, water, methanol, tert-butanol, tetrahydrofuran, toluene); (g) (h) Photographs of fluorescence changes of **S1** and **S2**.

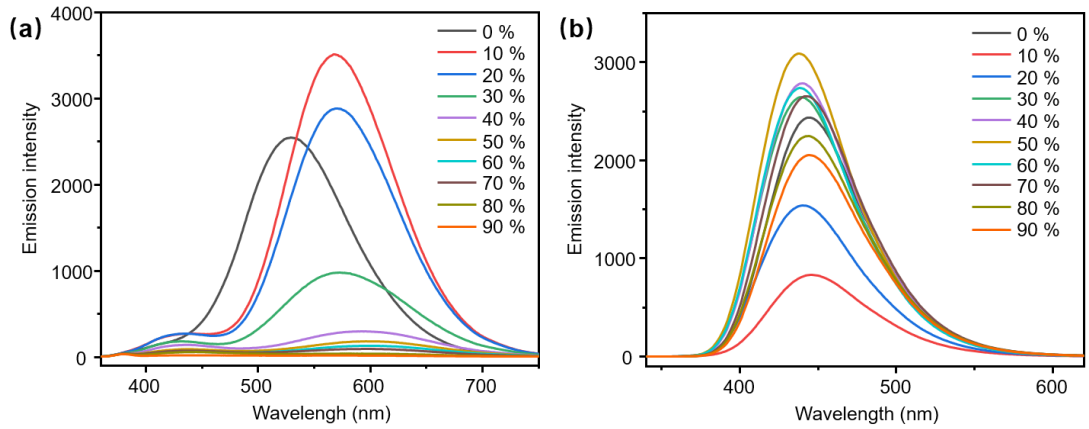

Figure S41. Fluorescence spectrum of (a) **L1** (λex = 340 nm, c = 1.0 μM) at PMT Voltage 500 V and (b) **L2** (λex = 340 nm, c = 1.0 μM) at PMT Voltage 400 V with various methanol content.

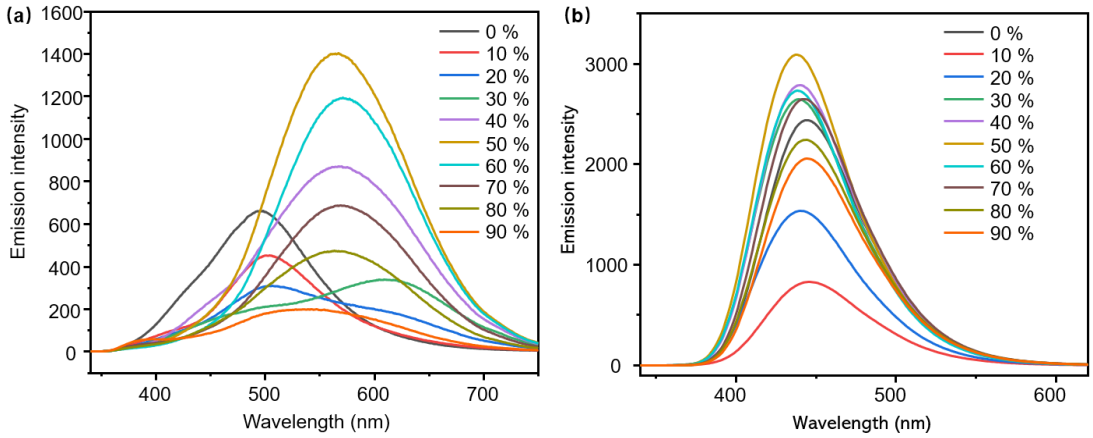

Figure S42. Fluorescence spectrum of (a) **S1** (λ_{ex} = 340 nm, c = 1.0 μM) at PMT Voltage 500 V and (b) **S2** (λ_{ex} = 340 nm, c = 1.0 μM) at PMT Voltage 350 V with various H_2O content.

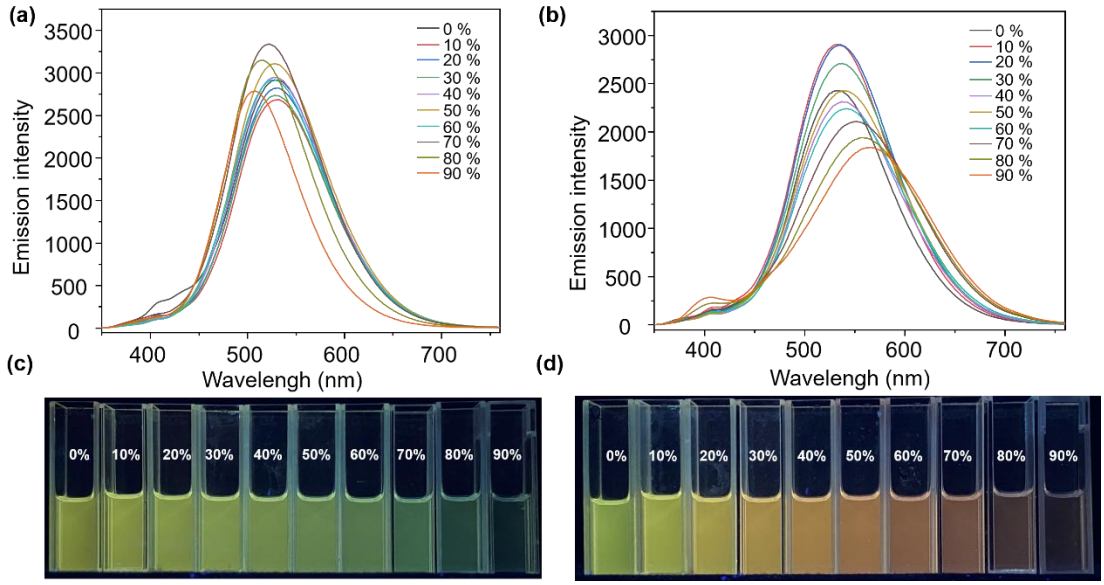

Figure S43. (a) (b) Fluorescence spectrum (λ_{ex} = 340 nm, c = 1.0 μM); (c) (d) photographs of **L1** in $CHCl_3$/1,4-dioxane and in $CHCl_3$/THF with various 1,4-dioxane or THF content.

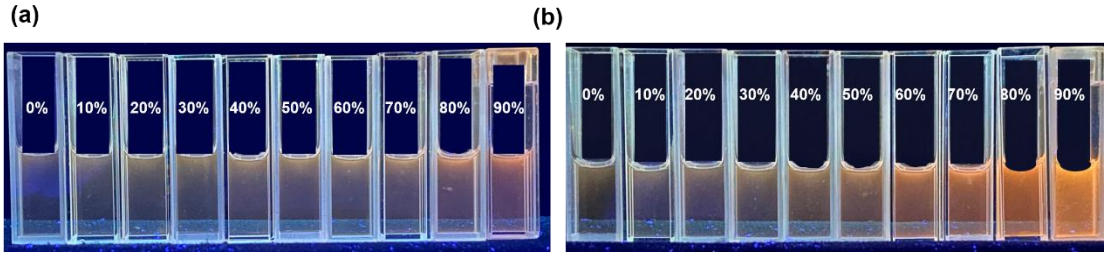

Figure S44. (a) photographs of **S1** in DMF/THF with various THF content, (b) (a) photographs of **S1** in DMF/tert-butanol with various tert-butanol content.

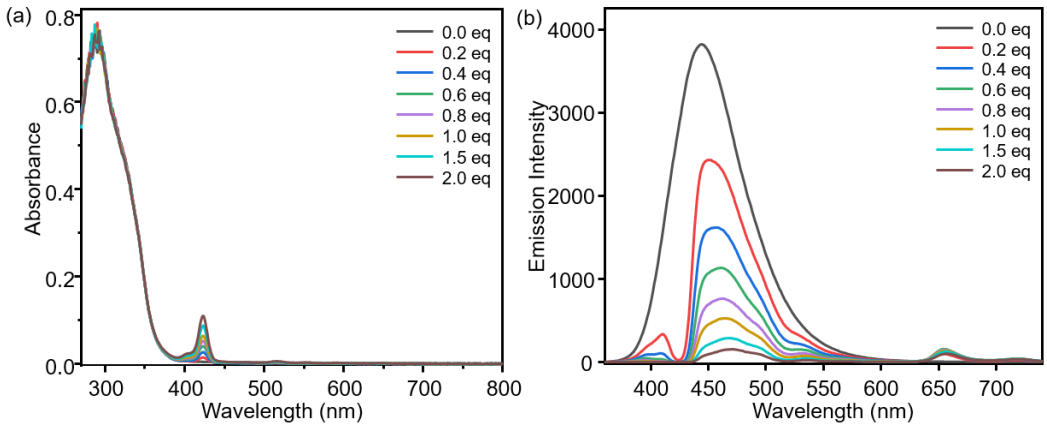

Figure S45. (a) UV-vis (0.5 μM in DMF) of free **S2** and different amounts of porphyrin were added to **S2**; (b) Emission (0.5 μM in DMF) of free **S2** and different amounts of porphyrin were added to **S2.**

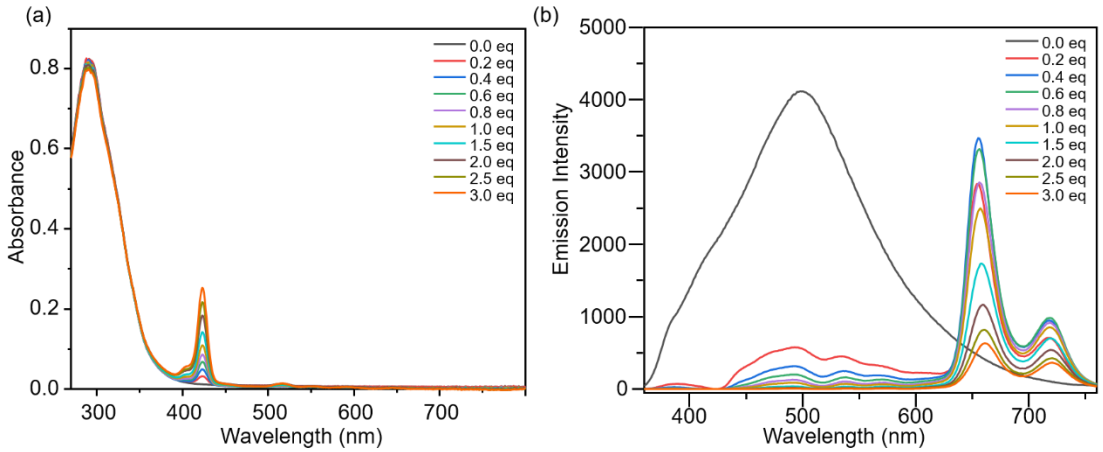

Figure S46. (a) UV-vis (0.5 μM in DMF) of free **S1** and different amounts of porphyrin were added to **S1**; (b) Emission (0.5 μM in DMF) of free **S1** and different amounts of porphyrin were added to **S1.**

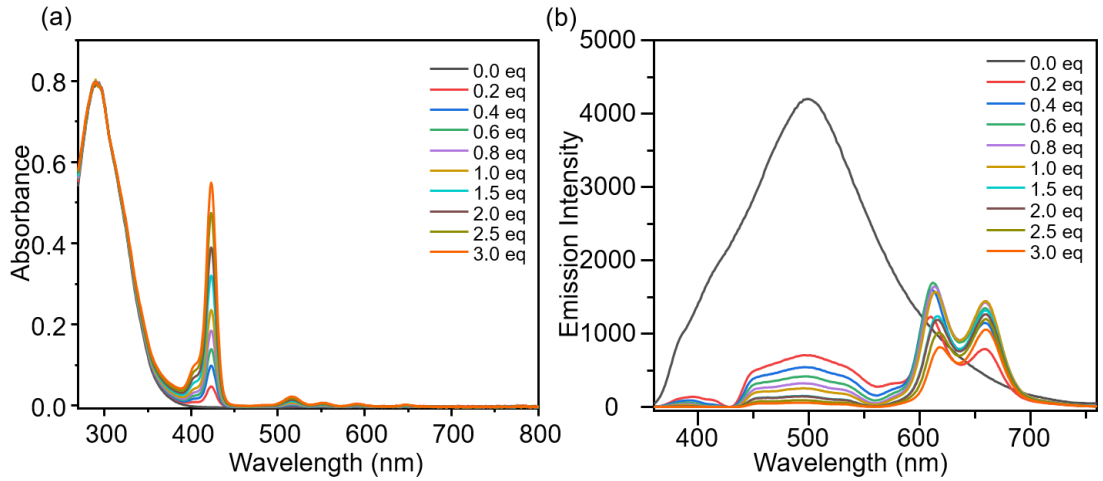

Figure S47. (a) UV-vis (0.5 μM in DMF) of free **S1** and different amounts of zinc porphyrin were added to **S1**; (b) Emission (0.5μM in DMF) of free **S1** and different amounts of zinc porphyrin were added to **S1.**

9. Crystallographic date of ligands

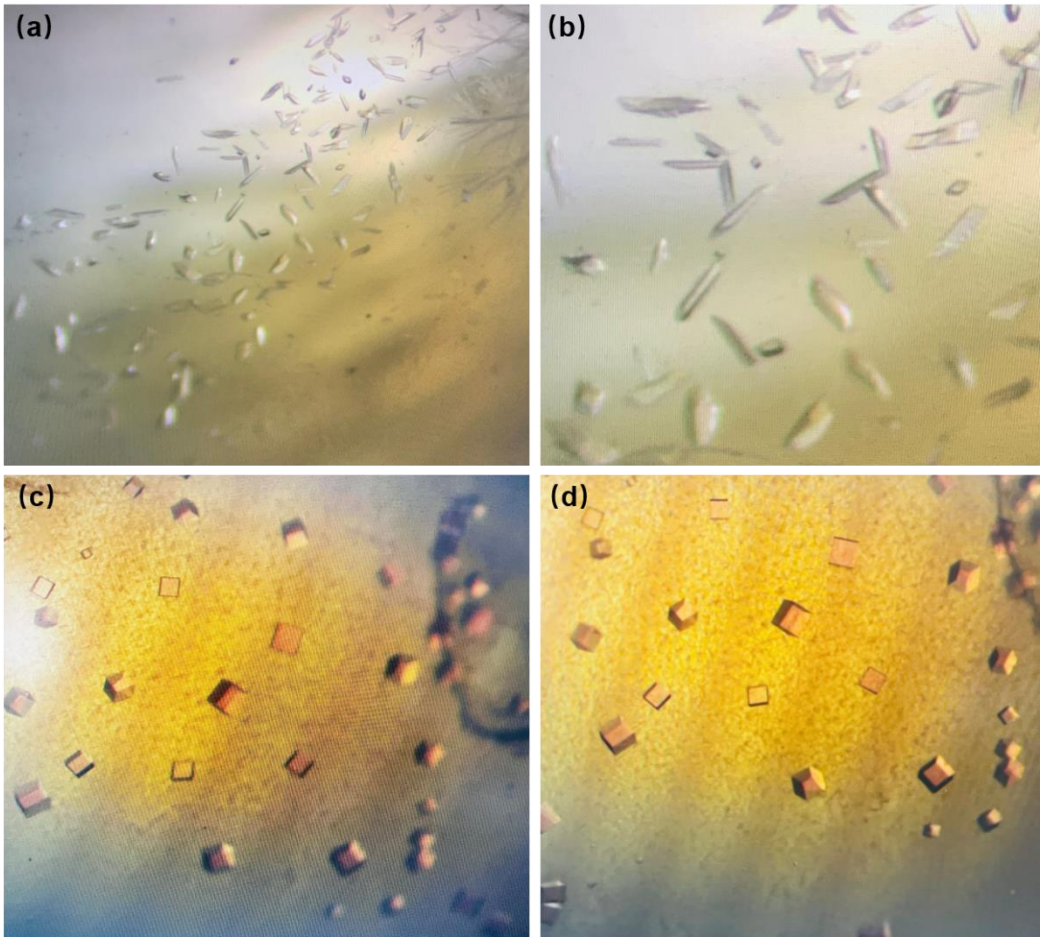

Figurer S48. The crystal structure photograph of (a) (b) **S1** and (c) (d) **S2**.

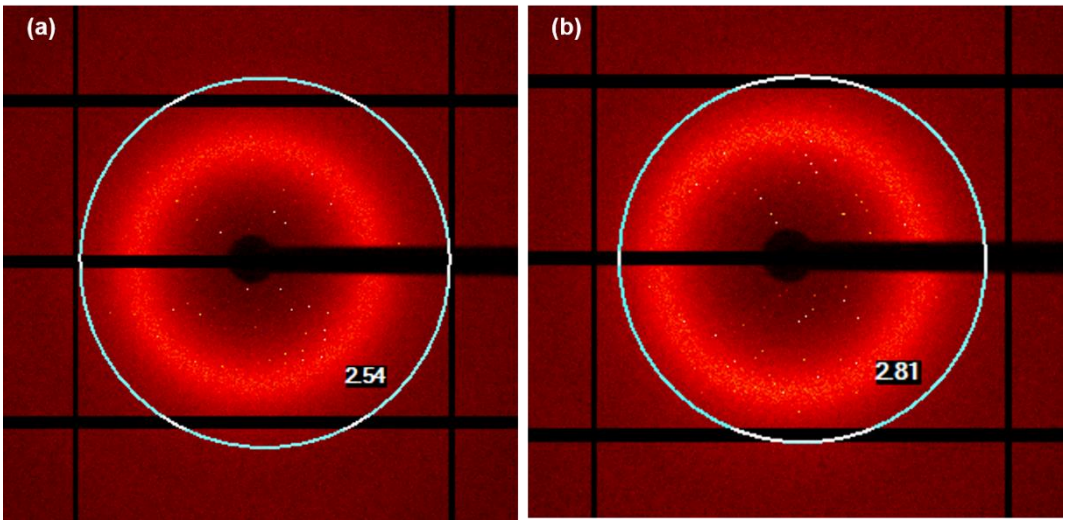

Figure S49. The diffraction points of the **S2** crystal.

Table S3. Crystallographic data of **L1, L2**

Identification code	Compound **L1**	Compound **L2**
CCDC number	2132604	2132525
Empirical formula	$C_{96}H_{60}N_{12}S_2$	$C_{96}H_{60}N_{12}O_4S_2$
Formula weight	1470.70	1504.73
Temperature/K	100(2) K	100(2) K
Crystal system	triclinic	monoclinic
Space group	*P-1*	*Cm*
Unit cell dimensions	a = 13.8636(3) Å b = 15.9137(3) Å c = 20.4987(4) Å α = 83.865(2)° β = 73.294(2)° γ = 85.019(2)°	a = 9.1813(8) Å b = 32.2736(14) Å c = 40.651(3) (4) Å α = 90° β = 96.354(8)° γ = 90°
Volume	4299.28(16) Å	11971.5(15)
Z	2	154
Density (calculated)	1.136 g/m^3	1.604 g/m^3
Absorption coefficient	0.115 mm^{-1}	0.767 mm^{-1}
F(000)	1530.0	5852.0
Crystal size	0.2 × 0.05 × 0. 05 mm^3	0.4 × 0.08 × 0. 08 mm^3
Radiation	Mo$K\alpha$ (λ = 0.71073)	Mo$K\alpha$ (λ = 0.71073)
Theta range for data collection	4.324 to 62.46°	4.638 to 62.348°
Index ranges	−19≤h≤19, −22≤k≤22, −29≤l≤28	-11≤h≤12, -43≤k≤43, -57≤l≤54
Reflections collected	70881	76442

Independent reflections	22440 [R_{int} = 0.0470, R_{sigma} = 0.0635]	28020 [R_{int} = 0.1854, R_{sigma} = 0.2404]
Data / restraints / parameters	22440/0/1004	28020/650/883
Goodness−of−fit on F^2	1.358	2.242
Final R indexes [I>=2σ (I)]	R_1 = 0.1209, wR_2 = 0.3490	R_1= 0.2743, wR_2 = 0.5503
Final R indexes [all data]	R_1 = 0.1655, wR_2 = 0.3759	R_1 = 0.4547, wR_2 = 0.5918
Largest diff. peak/hole	1.95/−0.41 e•Å^{-3}	3.03/-0.86 e•Å^{-3}
Flack parameter	-0.07(8)	-0.09(9)

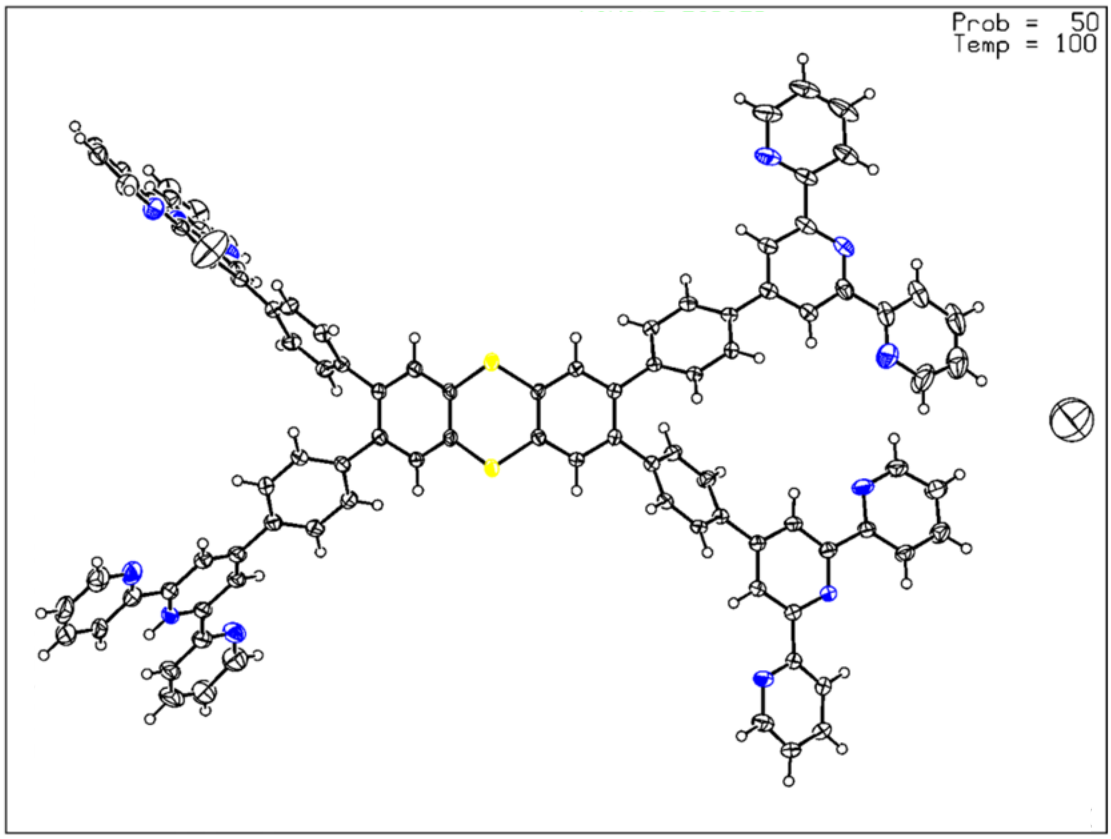

Figure S50. ORTEP Drawing of **L1**. The thermal ellipsoids are drawn at 50% probability

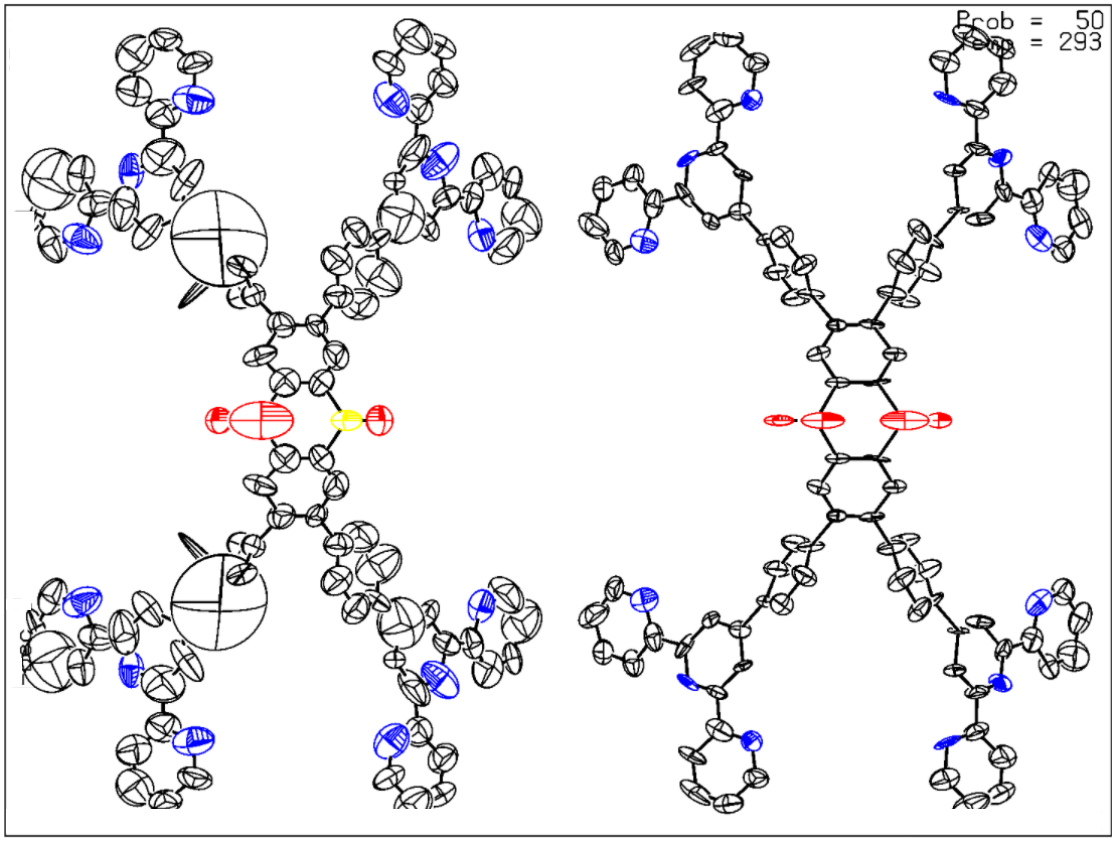

Figure S51. ORTEP Drawing of **L2**. The thermal ellipsoids are drawn at 50% probability

References

1. H. Gilman and D. Swayampati, *J. Org. Chem.*, 1958, **23**, 313-314.
2. T.-Z. Xie, J.-Y. Li, Z. Guo, J. M. Ludlow Iii, X. Lu, C. N. Moorefield, C. Wesdemiotis and G. R. Newkome, *Eur. J. Inorg. Chem.*, 2016, **11**, 1671-1677.
3. M. J. Aroney, R. J. W. Le Fèvre and J. D. Saxby, *J. Chem. Soc*, 1965, 571-575.
4. D. Casarini, C. Coluccini, L. Lunazzi and A. Mazzanti, *J. Org. Chem.*, 2006, **71**, 6248-6250.
5. B. P. Borah and J. Bhuyan, *J. Chem. Sci. (Bangalore, India)*, 2018, **130**, 117-125.
6. N. G. Singh, K. D. Borah, S. Majumder and J. Bhuyan, *J. Mol. Struct.*, 2020, **1200**, 127116-127124.
7. R. Soury, M. Chaabene, M. Jabli, T. A. Saleh, R. Ben Chaabane, E. Saint-Aman, F. Loiseau, C. Philouze, A.-R. Allouche and H. Nasri, *Chem. Eng. J.*, 2019, **375**, 122005-122019.
8. A. Kumari, *Z. Naturforsch.*, 2004, **59**, 615-620.
9. H. Wang, K. Wang, Y. Xu, W. Wang, S. Chen, M. Hart, L. Wojtas, L.-P. Zhou, L. Gan, X. Yan, Y. Li, J. Lee, X.-S. Ke, X.-Q. Wang, C.-W. Zhang, S. Zhou, T. Zhai, H.-B. Yang, M. Wang, J. He, Q.-F. Sun, B. Xu, Y. Jiao, P. J. Stang, J. L. Sessler and X. Li, *J. Am. Chem. Soc.*, 2021, **143**, 5826-5835.